JGP Journal of General Physiology

RESEARCH ARTICLE

Extracellular protons accelerate hERG channel deactivation by destabilizing voltage sensor relaxation

Yu Patrick Shi, Samrat Thouta, Yen May Cheng, and Tom W. Claydon

hERG channels underlie the delayed-rectifier K^+ channel current (I_{Kr}), which is crucial for membrane repolarization and therefore termination of the cardiac action potential. hERG channels display unusually slow deactivation gating, which contributes to a resurgent current upon repolarization and may protect against post-depolarization–induced arrhythmias. hERG channels also exhibit robust mode shift behavior, which reflects the energetic separation of activation and deactivation pathways due to voltage sensor relaxation into a stable activated state. The mechanism of relaxation is unknown and likely contributes to slow hERG channel deactivation. Here, we use extracellular acidification to probe the structural determinants of voltage sensor relaxation and its influence on the deactivation gating pathway. Using gating current recordings and voltage clamp fluorimetry measurements of voltage sensor domain dynamics, we show that voltage sensor relaxation is destabilized at pH 6.5, causing an ∼20-mV shift in the voltage dependence of deactivation. We show that the pH dependence of the resultant loss of mode shift behavior is similar to that of the deactivation kinetics acceleration, suggesting that voltage sensor relaxation correlates with slower pore gate closure. Neutralization of D509 in S3 also destabilizes the relaxed state of the voltage sensor, mimicking the effect of protons, suggesting that acidic residues on S3, which act as countercharges to S4 basic residues, are involved in stabilizing the relaxed state and slowing deactivation kinetics. Our findings identify the mechanistic determinants of voltage sensor relaxation and define the long-sought mechanism by which protons accelerate hERG deactivation.

Introduction

The human ether-à-go-go–related gene (hERG) encodes a voltage-gated potassium (Kv) channel that underlies the rapid delayed-rectifier K^+ channel current (I_{Kr}), which is crucial in the repolarization and termination of the human cardiac action potential (Sanguinetti et al., 1995). The gating kinetics of hERG channels are unique and underlie their physiological importance. Upon depolarization, the hERG channel activates slowly and inactivates rapidly, passing little current during the early phase of the action potential. Upon repolarization, the hERG channel recovers rapidly from inactivation into the open state from which deactivation is slow, permitting a resurgent current that aids repolarization of the cell. It is well established that inherited mutations or drug block that reduce hERG channel function result in compromised resurgent I_{Kr} current and delayed repolarization (Curran et al., 1995; Sanguinetti et al., 1995, 1996), which establishes a substrate for arrhythmogenesis. However, in addition to facilitating phase 3 action potential repolarization, slow deactivation of hERG channels may also maintain refractoriness of cardiac tissue during early diastole and protect against ectopic beats caused by triggered activity (Smith et al., 1996; Lu et al., 2001). This notion highlights the need to understand the mechanisms of slow deactivation and its role in protecting against triggered activity.

hERG channels share structural homology with other Kv channels, with six α-helical transmembrane segments (S1–S6) assembled in a tetrameric configuration with S1–S4 forming the voltage-sensing domain and S5–S6 forming the pore domain. Voltage sensitivity arises from the movement of basic S4 helix charges in response to changes in membrane voltage, which result in the translocation of 6–8 *e* per tetramer across the membrane (Zhang et al., 2004). Numerous studies have suggested that S4 charge movement is coupled to opening of the pore gate via the S4–S5 linker (Sanguinetti and Xu, 1999; Ferrer et al., 2006; Van Slyke et al., 2010; Hull et al., 2014); however, this has been chal-

Department of Biomedical Physiology and Kinesiology, Simon Fraser University, Burnaby, British Columbia, Canada.

Correspondence to Tom W. Claydon: thomas_claydon@sfu.ca.

lenged recently by the observation that the S4–S5 linker is short and not domain-swapped in cryo-electron microscopy (cryo-EM) structures of hERG channels (Wang and MacKinnon, 2017) and that coexpression of hERG channel halves, physically split within the S4–S5 linker, coassemble to produce WT-like channel activation gating (Lörinczi et al., 2015; de la Peña et al., 2018). Regardless of the mechanism of the coupling between voltage sensing and pore opening, measurement of the energetics of pore opening suggest that the open state of the pore is stable (ΔG_0 = −8.4 kJ mol^{-1}) and that work must be done to close the pore (Hardman et al., 2007; Cheng et al., 2013). This observation indicates deactivation gating as a key regulator of hERG channel open probability, which underscores the need to elucidate the mechanics of slow deactivation gating. Indeed, acceleration of deactivation kinetics is known to be associated with long QT syndrome type 2 (LQTS2) and sudden cardiac death (Chen et al., 1999).

Several regions within hERG channels have been associated with modulation of deactivation kinetics. Truncation of, or substitutions within, the N-terminus accelerate deactivation kinetics (Spector et al., 1996; Morais Cabral et al., 1998; Wang et al., 1998, 2000; Chen et al., 1999; Ng et al., 2011; Tan et al., 2012; Adaixo et al., 2013), and several studies using a variety of approaches have suggested that the N-terminus may stabilize the open state of the channel via interactions with the S4–S5 linker, the C-linker, and the C-terminal cyclic-nucleotide–binding homology domain (Al-Owais et al., 2009; Gustina and Trudeau, 2011, 2012; Ng et al., 2012, 2014; Brelidze et al., 2013; de la Peña et al., 2013, 2015). Together, these findings imply that deactivation is influenced by a complex gating machinery involving several cytoplasmic elements (Morais Cabral et al., 1998; Wang et al., 1998; Fernández-Trillo et al., 2011; Ng et al., 2012; de la Peña et al., 2013; Hull et al., 2014). However, numerous mutations throughout the channel transmembrane core also accelerate deactivation (Liu et al., 2003; Subbiah et al., 2004; Zhang et al., 2005; Van Slyke et al., 2010; Hull et al., 2014; Shi et al., 2014). In addition, extracellular ionic manipulations, e.g., increased protons or divalent cations, also accelerate deactivation kinetics (Anumonwo et al., 1999; Jiang et al., 1999; Johnson et al., 1999b; Terai et al., 2000; Bett and Rasmusson, 2003; Lin and Papazian, 2007; Abbruzzese et al., 2010; Shi et al., 2014). These observations invoke the need to understand the underlying deactivation regulatory mechanisms.

Recent studies suggest that voltage sensor relaxation contributes to slow deactivation in hERG channels (Tan et al., 2012; Goodchild and Fedida, 2014; Thouta et al., 2017). The mechanistic basis of relaxation is not fully understood, but it describes events following depolarization that further stabilize (relax) the voltage sensor in the activated configuration. Relaxation of the voltage sensor into this more stable state results in more energy being required to return the voltage sensor to its resting state upon repolarization than required to activate it. Thus, voltage sensor relaxation results in an energetic separation of the activation and deactivation pathways, producing a hysteresis, which has been previously described as a mode shift. Such mode shift behavior has been reported in numerous channels, such as Shaker (Haddad and Blunck, 2011; Lacroix et al., 2011; Labro et al., 2012; Priest et al., 2013), Kv1.2 (Labro et al., 2012), NaChBac (Kuzmenkin et al., 2004), HCN (Elinder et al., 2006; Xiao et al., 2010), L-type calcium (Brum et al., 1987, 1988), and Hv1 (Villalba-Galea, 2014), as well as in the voltage sensor–related protein *Ci*-VSP (Villalba-Galea et al., 2008), and these observations have led to the suggestion that mode shift due to relaxation is an intrinsic property of the channel voltage sensor. Importantly, however, although in most cases mode shift requires prolonged depolarization, mode shift in hERG channels occurs in response to depolarizations that are of physiologically relevant duration (Goodchild et al., 2015; Thouta et al., 2017). As such, pore closure is slowed by relatively brief occupancy of the open channel state. We recently demonstrated that membrane depolarization stabilizes the hERG voltage sensor in the relaxed state, increasing the energy required for charge return, and that partial return of charge appears to trigger closure of the pore gate (Thouta et al., 2017). Accordingly, we hypothesize that entry of the voltage sensor into a stable relaxed state limits channel closing and that, upon repolarization, transition of an individual subunit voltage sensor back to rest triggers closure of the pore via the S4–S5 linker and other cytoplasmic elements to regulate channel deactivation.

In the current study, we use external acidification as a tool to demonstrate a connection between voltage sensor relaxation and the kinetics of deactivation in hERG channels. Using two methods to track voltage sensor measurement, we show that acidic pH attenuates voltage sensor relaxation, indicating that both approaches are reliable in tracking voltage sensor reconfigurations and that low pH destabilizes the relaxed state of the voltage sensor by lowering the energetic landscape for its return. Furthermore, we identify D509 in S3 as a proton sensor site that resides in a dynamic region of the hERG cryo-EM structure and is important in mediating the sensitivity of relaxation to external protons. In doing so, we identify a site and mechanism of action of the well-known proton-induced acceleration of hERG channel deactivation gating. These findings provide a description of the molecular mechanism that regulates deactivation gating in hERG channels.

Materials and methods

Molecular biology

hERG1a channel cDNA was subcloned into a pBluescript SKII expression vector. The D509A mutation was generated by conventional overlap extension PCR. Mutagenic primers were synthesized by Sigma-Genosys. The mutation was confirmed by sequencing using Eurofins MWG Operon. The XbaI restriction enzyme was used to linearize the construct for subsequent synthesis of cRNA with the mMessage mMachine T7 Ultra cRNA Transcription Kit (Ambion).

Oocyte preparation and injection

In agreement with the policies and procedures of the Simon Fraser University Animal Care Committee and the Canadian Council of Animal Care, *Xenopus laevis* frogs were terminally anaesthetized by immersion in 2 g liter^{-1} tricaine solution for 25 min, and oocyte lobes were surgically removed. Oocyte lobes were treated with collagenase (1 mg ml^{-1} collagenase type 1A in MgOR2 solution [in mM: 96 NaCl, 2 KCl, 20 $MgCl_2$, and 5 HEPES, titrated to pH 7.4 with NaOH]) for 1 h before manual defolliculation and iso-

lation of stage V–VI oocytes. Defolliculated oocytes were injected with 50 nl cRNA using a Drummond digital microdispenser and stored in SOS$^+$ media (in mM: 96 NaCl, 2 KCl, 1.8 $CaCl_2$, 1 $MgCl_2$, 5 HEPES, 5% horse serum, 2.5 sodium pyruvate, and 100 mg liter^{-1} gentamicin sulfate, titrated to pH 7.4 with NaOH) at 19°C for 1–3 d before recording.

Electrophysiology

All recordings were performed at 20–22°C. Ionic current recordings were performed using conventional two-electrode voltage clamp with an OC-725C amplifier (Warner Instruments) coupled to a Digidata 1440 interface (Axon Instruments). Oocytes were bathed in ND96 solution containing (in mM) 96 NaCl, 3 KCl, 0.5 $CaCl_2$, 1 $MgCl_2$, and 5 HEPES, titrated to pH 7.4 or 6.5 with NaOH. HEPES was replaced by Mes in solutions more acidic than pH 6.5. All reagents were purchased from Sigma-Aldrich. Experiments were performed under constant perfusion (1 ml min^{-1}), and complete exchange of bath solution titrated to different pH was achieved following 5-min perfusion before recordings. Glass recording microelectrodes were made with thin-walled borosilicate glass (World Precision Instruments) and when filled with 3 M KCl had a tip resistance of 0.2–0.8 MΩ. All current signals were acquired with a 10-kHz sampling frequency and were low-pass filtered at 4 kHz (–3 dB, 8-pole Bessel filter).

Gating currents were measured using the cut-open Vaseline gap technique with a CA-1B amplifier (Dagan) and recorded by Patchmaster software (ITC-16 interface; HEKA Electronik). External gating solution consisted of (in mM) 120 tetraethylammonium hydroxide (TEA-OH), 120 Mes, 0.5 Ca-Mes, and 10 HEPES (titrated to pH 7.4 or pH 6.5 using Mes). Internal gating solution consisted of (in mM) 120 TEA-OH, 120 Mes, 2 EGTA, and 10 HEPES (titrated to pH 7.4). Oocytes were permeabilized by a 30–60-s application of internal gating current solution supplemented by 0.1% saponin. Following permeabilization, but before gating current recordings, cells were held at –10 mV for 30 min to deplete cytosolic K$^+$ and to minimize ionic currents. The hERG channel blocker terfenadine (20 μM) was added in both external and internal gating solutions to inhibit residual hERG ionic currents. Glass recording microelectrodes were made from thin-walled borosilicate glass and had a resistance of 250–500 kΩ when filled with 3 M CsCl. Capacitive currents were subtracted using the analogue circuitry of the amplifier; linear leak subtraction was performed online using a P/–8 protocol. We were unable to resolve gating currents in oocytes expressing hERG D509A channels. This is likely due to lower expression levels of these mutant channels compared with WT; while we were able to resolve fluorescence recordings from the L520C reporter site (see below) in D509A channels, signals were consistently smaller than in the absence of the D509A mutation.

Voltage clamp fluorimetry

The L520C mutation was introduced in the N-terminal S4 segment (extracellularly accessible) to engineer a labeling site for tetramethylrhodamine-5-maleimide (TMRM; Invitrogen Life Technologies). Two native cysteines in the S1–S2 extracellular linker (C445 and C449) were also mutated to valine to reduce nonspecific labeling. Oocytes were labeled in the dark with depolarizing solution (in mM: 98 KCl, 1 $MgCl_2$, 2 $CaCl_2$, and 5 HEPES, titrated to pH 7.4 with NaOH) supplemented with 5 μM TMRM for 30 min at 10°C and then washed with ND96 solution. Two-electrode voltage clamp fluorimetry was performed with a Nikon TE2000S inverted microscope (Nikon Canada) with an epifluorescence attachment and photomultiplier tube detection module (Cairn Research) as described previously (Van Slyke et al., 2010).

Data analysis

Data acquisition and analysis were performed using pClamp 10.2 (Axon Instruments), SigmaPlot 11 (Systat Software), or IGOR Pro 6 (WaveMetrics) software. Activation and deactivation G-V were measured from peak tail currents obtained upon repolarization from a series of test voltages. Measurements of charge displacement (Q) vs. voltage (Q-V relationships) for activation and deactivation were obtained by integrating the off-gating currents at –100 mV (Ig_{off}) and on-gating currents at 0 mV for 500 ms (Ig_{on}), respectively, elicited by step changes in test voltage. In this way, charge movement during the fixed duration at the standard off- or on-test voltage is used as a measure of the total charges moved in the preceding, variable conditioning pulse, as has been performed previously (Piper et al., 2003; Goodchild and Fedida, 2014; Thouta et al., 2017). Measurements of fluorescence–voltage relationships (F-V) for activation and deactivation were obtained by measuring the fluorescence change at the end of each voltage step. G-V, Q-V, and F-V were plotted and fitted to the Boltzmann function: $y = 1/\{1 + \exp[(V_{1/2} - V)/k]\}$, where y is the normalized peak conductance, gating charge, or fluorescence change, $V_{1/2}$ is the half-activation potential, V is the variable (test) voltage, and k is the slope factor. Deactivation kinetics were quantified by fitting the decaying portion of the tail current during the test pulse to a biexponential function: $I = A_{fast}\exp(t/\tau_{fast}) + A_{slow}\exp(t/\tau_{slow}) + C$, where A_{fast} and A_{slow} are the amplitudes of the fast and slow components, τ_{fast} and τ_{slow} are the time constants for fast and slow components, and C is the residual amplitude. *pKa* values were calculated using the Hill equation: $y = \text{base} + (\text{max} - \text{base})/[1 + (K_a/[H^+])^n]$, where y is the fractional conductance, base and max are the minimum and maximum fractional current amplitudes, respectively, $[H^+]$ is the concentration of H$^+$, and n is the Hill coefficient. All data are expressed as mean ± SEM. Statistical comparisons between means were conducted using a two-tailed Student's t testor two-way ANOVA test, as appropriate, with $P < 0.05$ taken as an indicator for statistical significance.

Online supplemental material

Fig. S1 shows that the use of a hyperpolarized holding potential allows capture of the full F-V from TMRM labeling of L520C. Fig. S2 shows ionic current recordings and plots of the voltage dependence of activation and deactivation from hERG L520C C-less channels. Table S1 shows the effect of holding potential on F-V and G-V Boltzmann fit parameters.

Results

Acidic pH reduces mode shift behavior in hERG channels

Mode shift behavior reflects energetic separation of activation and deactivation gating and becomes pronounced in numer-

ous channels following prolonged depolarization (Piper et al., 2003; Elinder et al., 2006; Bruening-Wright and Larsson, 2007; Villalba-Galea et al., 2008; Haddad and Blunck, 2011; Lacroix et al., 2011; Labro et al., 2012; Hull et al., 2014; Villalba-Galea, 2014; Goodchild et al., 2015; Thouta et al., 2017). In hERG channels, robust mode shift behavior is evident following depolarization durations in the normal physiological range (Piper et al., 2003; Goodchild and Fedida, 2014; Thouta et al., 2017). This can be seen in Fig. 1 (A and B), which shows typical families of hERG channel currents recorded in response to voltage protocols used to measure the voltage dependence of activation and deactivation gating with physiological durations. We applied 250-ms depolarizing steps to measure activation and 750-ms repolarizing steps (following a 250-ms depolarization) to measure deactivation, so as to mimic durations typical of a basic cardiac cycle, although it should be noted that experiments were conducted at room temperature, not at physiological temperature. Boltzmann fits of normalized peak tail currents (Fig. 1 B) yielded $V_{1/2}$ values of −12.4 ± 1.1 mV for activation and −66.0 ± 0.9 mV for deactivation (n = 6). These data demonstrate that at physiological durations hERG channels display a robust mode shift with a voltage dependence of channel deactivation that is separated by −53.6 ± 1.8 mV from that of activation gating (Table 1).

We recently showed that the magnitude of mode shift is strongly dependent on experimental protocol duration and that the slow kinetics of hERG channel deactivation contributes to the generation of the mode shift measured using short step durations, such as those in Fig. 1 (Thouta et al., 2017). To further demonstrate this, we investigated the effect of acidic pH on mode shift behavior, since it is well known that external acidification accelerates hERG channel deactivation, albeit via an unknown mechanism (Anumonwo et al., 1999; Bérubé et al., 1999; Terai et al., 2000; Bett and Rasmusson, 2003; Liu et al., 2003; Zhou and Bett, 2010; Shi et al., 2014). Fig. 1 C shows typical current families recorded in response to the voltage protocols shown in Fig. 1 A with the external pH titrated to pH 6.5, which is within the pathophysiological range (Orchard and Cingolani, 1994) and accelerated deactivation kinetics. Normalized G-V for activation and deactivation derived from data such as these are shown in Fig. 1 D. We observed that while the $V_{1/2}$ of activation gating was only minimally affected (−5.9 ± 0.7 mV), the $V_{1/2}$ of deactivation gating (−43.0 ± 0.7 mV) was right shifted by +23 mV. These data suggest that mode shift behavior is correlated with deactivation kinetics and prompted us to investigate this relationship further.

The data shown in Fig. 1 suggest that acidic pH changes in this range alter the energy landscape experienced during deactivation to a greater extent than during activation gating, which is consistent with the observation that low pH markedly accelerates deactivation kinetics. To better understand the relationship between accelerated deactivation kinetics and the reduction in mode shift at low pH, we measured deactivation kinetics and mode shift using voltage steps long enough in duration to approximate steady state activation and deactivation voltage dependencies over a range of pH values (pH 8.5 to 4.5). Fig. 2 (A–C) shows the acceleration of deactivation kinetics with changes in external pH following a 15-s depolarizing step. Tail currents at −110 mV were fitted with a double exponential, and the resultant values for τ_{fast} are plotted against pH. A fit of the data with the Hill equation revealed that acidic pH accelerated deactivation kinetics with a *pKa* of pH 6.8 (n = 1.9), similar to that reported previously from shorter-duration steps (Bett and Rasmusson, 2003). We then measured the pH dependence of the mode shift behavior (Fig. 2, D–F) using long duration steps that allow slow activation and deactivation to reach close to steady state, as described previously (Thouta et al., 2017). Fig. 2 F plots the pH dependence of the mode shift fit to the Hill equation, which yielded a *pKa* of pH 7.0 (n = 1.1; see Table 2). The similarity in the pH dependence of deactivation kinetics (Fig. 2 C) and mode shift (Fig. 2 F) supports the hypothesis that accelerated deactivation kinetics reduce the measured mode shift behavior (Thouta et al., 2017). The Hill coefficient (n) values suggest that there may be some cooperativity in the interactions with protons that govern the kinetics of deactivation, which is consistent with the idea that deactivation involves downstream cytoplasmic interactions.

Acidic pH destabilizes the relaxed state of the voltage sensor

We next considered the mechanism by which external protons accelerate hERG channel deactivation kinetics. Previous evidence has suggested that acidic pH accelerates return of the voltage sensor domain (Es-Salah-Lamoureux et al., 2010; Van Slyke et al., 2010). In addition, stabilization of the activated voltage sensor in the relaxed state has been shown to slow hERG channel closing (Tan et al., 2012; Goodchild et al., 2015; Thouta et al., 2017). We hypothesized that external protons accelerate deactivation by destabilizing the relaxed state of the voltage sensor. Relaxation is likely an intrinsic property of the voltage sensor since the relaxation process is abolished following uncoupling of the pore from the voltage sensor domain in Shaker (Haddad and Blunck, 2011) and preserved in the absence of a pore in the isolated voltage sensor, *Ci*-VSP (Villalba-Galea et al., 2008). We therefore measured voltage sensor movement in hERG channels to directly investigate the effects of external protons on voltage sensor domain relaxation. Fig. 3 shows data from two different approaches that we used to report voltage sensor movement. A–C show recordings of hERG gating currents, which reflect charge movement, and D–F display measurements of fluorescence changes from a TMRM reporter tag attached to L520C at the outer end of the S4 segment, which reports on environmental changes during voltage sensor gating. We used both approaches to track voltage sensor behavior using long durations that allow near steady state equilibria of channels between activated and relaxed states. Fig. 3 A shows typical gating current recordings measured in response to the voltage protocol designed to assess activation (holding potential, −100 mV). Boltzmann fits of the data yielded a $V_{1/2}$ value of −48.2 ± 0.5 mV (n = 3) for the Q_{on}-V (see Materials and methods). Fig. 3 B shows typical gating current recordings measured in response to the voltage protocol designed to assess deactivation (holding potential, 0 mV). The fit of the Q_{off}-V yielded a $V_{1/2}$ value of −75.5 ± 2.3 mV (n = 4). From these data recorded using voltage steps long enough in duration to allow measurement of near steady state equilibria, the mode shift of the voltage sensor was −27.3 ± 2.4 mV. These data reflect the entry of the hERG voltage sensor into a stable relaxed state upon depolarization.

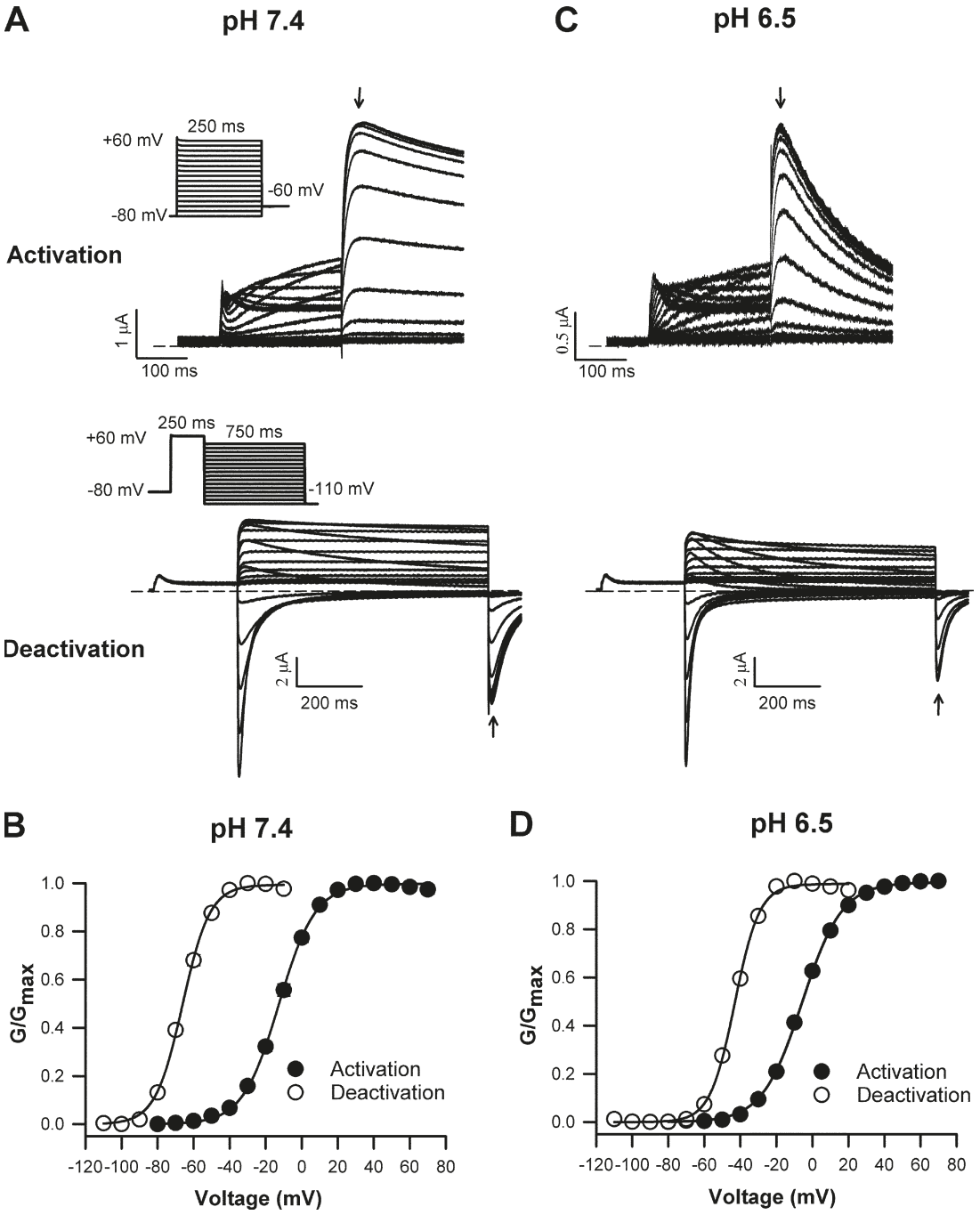

Figure 1. **hERG mode shift is reduced by acidic pH. (A)** Typical ionic recordings elicited with activating voltage-step durations of 250 ms and deactivating voltage-step durations of 750 ms (following depolarization to +60 mV for 250 ms), mimicking physiological durations of a cardiac action potential. Arrows mark where current measurements were made. **(B)** Plots of the normalized G-V for activation and deactivation, fitted to a Boltzmann function, yielded $V_{1/2}$ values of −12.4 ± 1.1 mV and −66.0 ± 0.9 mV, respectively. The mean mode shift was −53.6 ± 1.8 (n = 6). **(C)** Typical ionic recordings from the activation and deactivation protocols in A at pH 6.5. **(D)** Boltzmann fits of the normalized G-V for activation and deactivation yielded $V_{1/2}$ values of −5.9 ± 0.7 mV and −43.0 ± 0.7 mV, respectively, with a mode shift of −37.1 ± 1.1 mV (n = 6), which was reduced by 31% compared with that at pH 7.4 ($P < 0.0001$, Student's t test). Dashed lines represent baseline.

Voltage clamp fluorimetry reports of voltage sensor movement revealed very similar findings to those of charge movement. We recorded fluorescence reports during hERG channel activation and deactivation using the same near-steady state durations as those used above to record gating currents. We used TMRM as a fluorescence reporter attached to a cysteine residue engineered at L520 on top of the S4 voltage sensor (with the native C445 and C449 cysteines in the S1–S2 linker mutated to valine). Some question has been raised over the suitability of this site as a reporter of voltage sensor movement, largely due to the observation that the F-V overlays the G-V rather than the Q-V; however, introduction of a brief prepulse to −120 mV in the volt-

Table 1. **Activation and deactivation G-V Boltzmann fit parameters recorded with physiological durations**

	Activation G-V $V_{1/2}$ (mV)	*k*	Deactivation G-V $V_{1/2}$ (mV)	*k*	Mode shift $V_{1/2}$ (mV)
WT					
pH 7.4	−12.4 ± 1.1 (6)	9.9 ± 0.4	−66.0 ± 0.9 (6)	7.3 ± 0.2	−53.6 ± 1.8
pH 6.5	−5.9 ± 0.7 (6)	11.2 ± 0.3	−43.0 ± 0.7 (6)	6.4 ± 0.1	−37.1 ± 1.1
D509A					
pH 7.4	+17.1 ± 0.8 (5)	14.7 ± 0.4	+1.6 ± 1.1 (5)	12.0 ± 0.4	−15.5 ± 1.4
pH 6.5	+21.6 ± 1.5 (5)	15.1 ± 0.2	+4.8 ± 1.2 (5)	11.6 ± 0.3	−16.8 ± 1.9

Data are expressed as mean ± SEM, with the number of cells in parentheses.

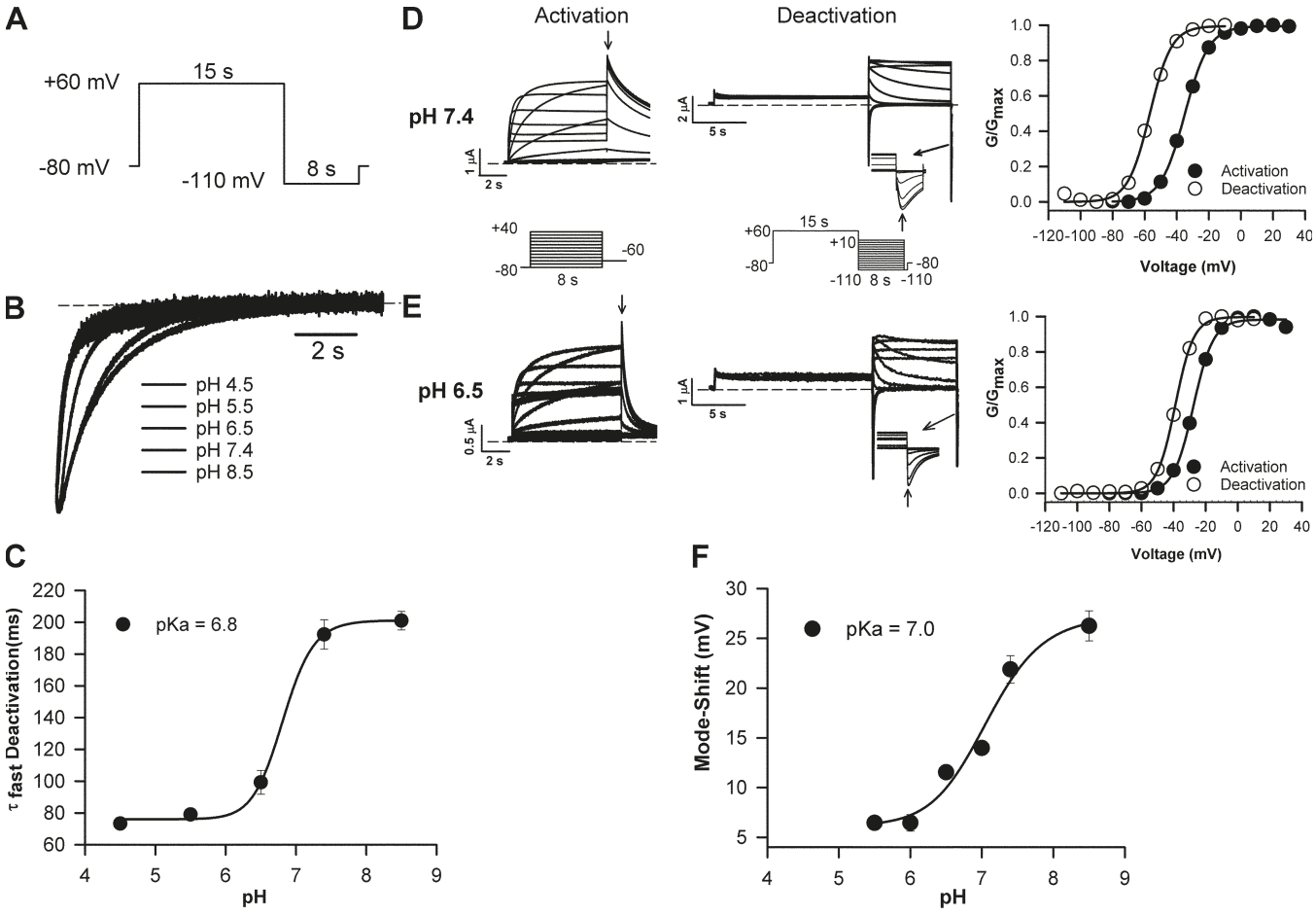

Figure 2. **The pH sensitivity of mode shift behavior is similar to that of deactivation kinetics. (A and B)** hERG channels were recruited into the relaxed state by applying a 15-s depolarizing step to +60 mV, following which deactivation kinetics were assessed during a repolarizing step to −110 mV. Current decay during repolarization was fitted to exponential function, which yielded values for τ_{fast} of 201 ± 11 ms (pH 8.5, *n* = 4), 192 ± 20 ms (pH 7.4, *n* = 5), 99 ± 16 ms (pH 6.5, *n* = 5), 79 ± 5 ms (pH 5.5, *n* = 5), and 73 ± 7 ms (pH 4.5, *n* = 5). **(C)** Plot of the pH dependence of the τ_{fast} of deactivation. Fitting the data with a Hill function yielded a *pKa* of pH 6.8 (Hill coefficient, *n* = 1.9). **(D and E)** Representative traces recorded during the voltage protocols (insets) designed to measure the steady state voltage dependence of activation and deactivation at pH 7.4 (D) and pH 6.5 (E). Arrows mark where current measurements were made. Plots of the normalized voltage dependence of activation and deactivation G-V at each pH are shown at right. Boltzmann fits of the data recorded at pH 7.4 yielded $V_{1/2}$ values for activation and deactivation of −34.5 ± 1.3 mV and −56.4 ± 1.2 mV, respectively (*n* = 12). Corresponding values measured at pH 6.5 were −27.3 ± 0.8 mV and −38.8 ± 1.2 mV (*n* = 5). The mode shift calculated from these data was reduced by 74% from −21.9 ± 1.4 mV at pH 7.4 to −11.5 ± 0.5 mV at pH 6.5. **(F)** Plot of the pH dependence of the mode shift measured as in D and E. Fitting the data with a Hill function yielded a *pKa* of pH 7.0 (Hill coefficient, *n* = 1.1; also see Table 2). Dashed lines represent baseline.

age protocol ensures complete return of the voltage sensor and the full capture of fluorescence change, yielding an F-V that is consistent with charge movement (Fig. S1 and Table S1). Fig. 3 (D and E) shows typical on- and off-fluorescence reports recorded in response to the voltage protocols shown. The $V_{1/2}$ of the F_{on}-V relationship was −44.7 ± 1.0 mV (*n* = 4), and that of the F_{off}-V was

Table 2. **pH dependence of steady state activation and deactivation G-V Boltzmann fit parameters**

WT	Activation G-V $V_{1/2}$ (mV)	*k*	Deactivation G-V $V_{1/2}$ (mV)	*k*	Mode shift $V_{1/2}$ (mV)
pH 8.5	−41.8 ± 0.8 (5)	7.5 ± 0.2	−68.1 ± 1.5 (5)	6.6 ± 0.3	−26.2 ± 1.5
pH 7.4	−34.5 ± 1.3 (12)	7.0 ± 0.3	−56.4 ± 1.2 (12)	6.5 ± 0.3	−21.9 ± 1.4
pH 7.0	−27.4 ± 0.9 (5)	8.1 ± 0.6	−41.4 ± 0.6 (5)	5.4 ± 0.5	−13.9 ± 0.5
pH 6.5	−27.3 ± 0.8 (5)	6.3 ± 0.9	−38.8 ± 1.2 (5)	6.2 ± 1.0	−11.5 ± 0.5
pH 6.0	−22.9 ± 1.8 (5)	7.7 ± 0.5	−29.3 ± 1.2 (5)	6.8 ± 0.7	−6.5 ± 0.8
pH 5.5	−11.5 ± 2.4 (4)	11.9 ± 0.5	−17.9 ± 2.2 (4)	6.9 ± 0.3	−6.4 ± 0.6

Data are expressed as mean ± SEM, with the number of cells in parentheses.

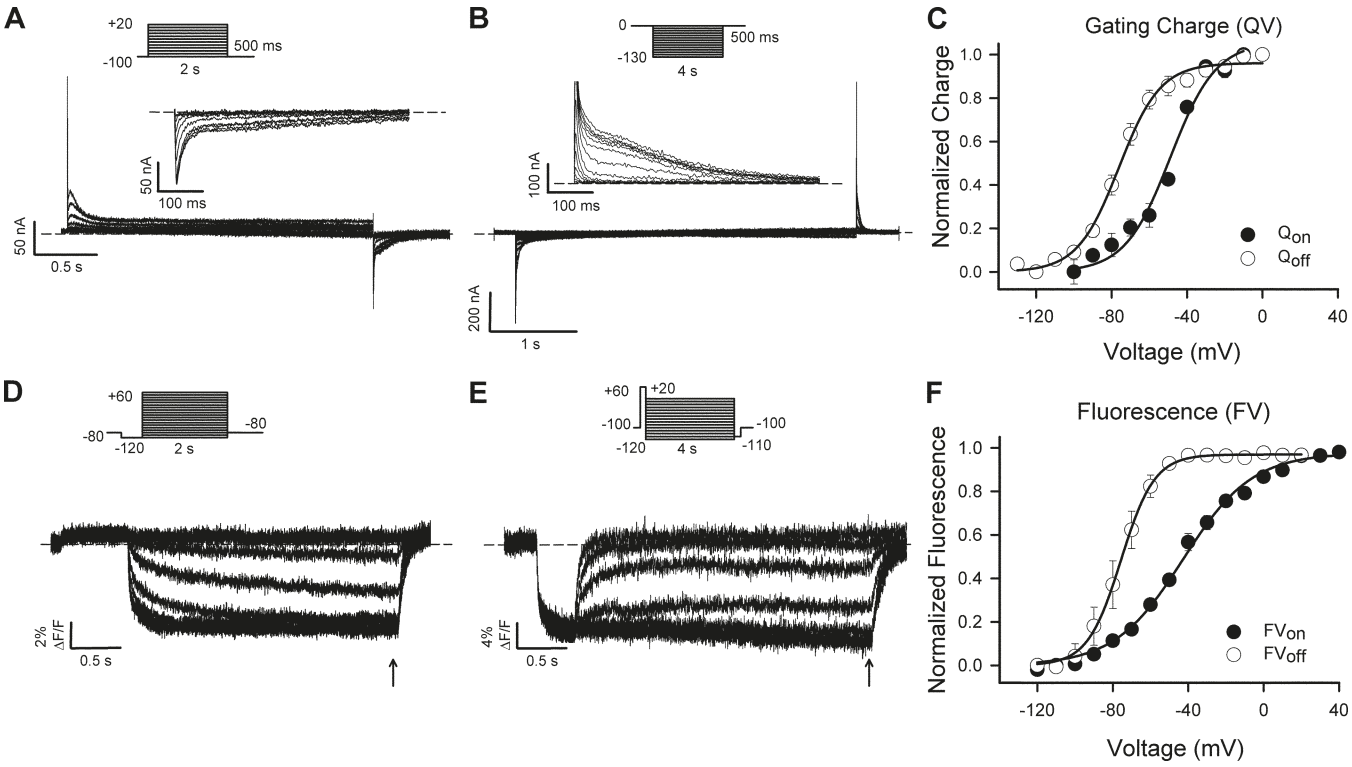

Figure 3. **Voltage sensor mode shift. (A and B)** Typical on-gating (Ig_{on}; A) and off-gating (Ig_{off}; B) currents recorded at pH 7.4 in response to the voltage protocol shown (insets). **(C)** Plot of the voltage dependence of Q_{on} and Q_{off}. Q_{on}-V was calculated from the integral of the off-gating current measured during a 500-ms step to −100 mV (A, inset). Q_{off}-V was determined from integrals of the on-gating current measured during a 500-ms step to 0 mV (B, inset). Data were fitted with a Boltzmann function, which yielded $V_{1/2}$ values for Q_{on} and Q_{off} of −48.2 ± 0.5 mV (n = 3) and −75.5 ± 2.3 mV (n = 4), respectively. The mean gating mode shift was −27.3 ± 2.4 mV. **(D and E)** Typical on-fluorescence (F_{on}; D) and off-fluorescence (F_{off}; E) reports from TMRM attached at L520C at pH 7.4 in response to the voltage protocols shown (insets). **(F)** Plot of the voltage dependence of normalized F_{on} and F_{off}. F_{on}-V was constructed by measuring relative fluorescence change at the end of the 2-s depolarizing voltage step. F_{off}-V was constructed by measuring relative fluorescence change at the end of the 4-s repolarizing voltage step. Data were fitted with a Boltzmann function, which yielded $V_{1/2}$ values for F_{on} and F_{off} of −44.7 ± 1.0 mV (n = 4) and −76.1 ± 3.2 mV (n = 5), respectively. The mean fluorescence mode shift was −31.4 ± 3.4 mV. The mean $V_{1/2}$ values measured for Q_{on} and F_{on} were not statistically different ($P > 0.17$), nor were the equivalent values for Q_{off} and F_{off} ($P > 0.74$). Dashed lines represent baseline.

−76.1 ± 3.2 mV (n = 5). These values are consistent with those measured for charge movement (Fig. 3 C) and report a similar voltage sensor mode shift of −31.4 ± 3.4 mV ($P > 0.05$, Student's t test) compared with the voltage sensor mode shift measured from gating charge. These data show that gating charge movement and fluorescence measurements of voltage sensor environmental change both report on the same relaxation-induced stabilization of the activated voltage sensor that results in voltage sensor mode shift.

To test our hypothesis that protons accelerate deactivation gating by destabilizing the relaxed state of the voltage sensor, we measured the effect of acidic pH on voltage sensor mode shift using gating current recordings and voltage clamp fluorimetry. We used the same voltage protocols as in Fig. 3 to ensure that recordings were made at near–steady state durations. Typical on- and off-gating current recordings at pH 6.5 are shown in Fig. 4 (A and B), and on- and off-fluorescence reports from L520C at pH 6.5 are shown in Fig. 4 (D and E). These recordings yielded $V_{1/2}$ values

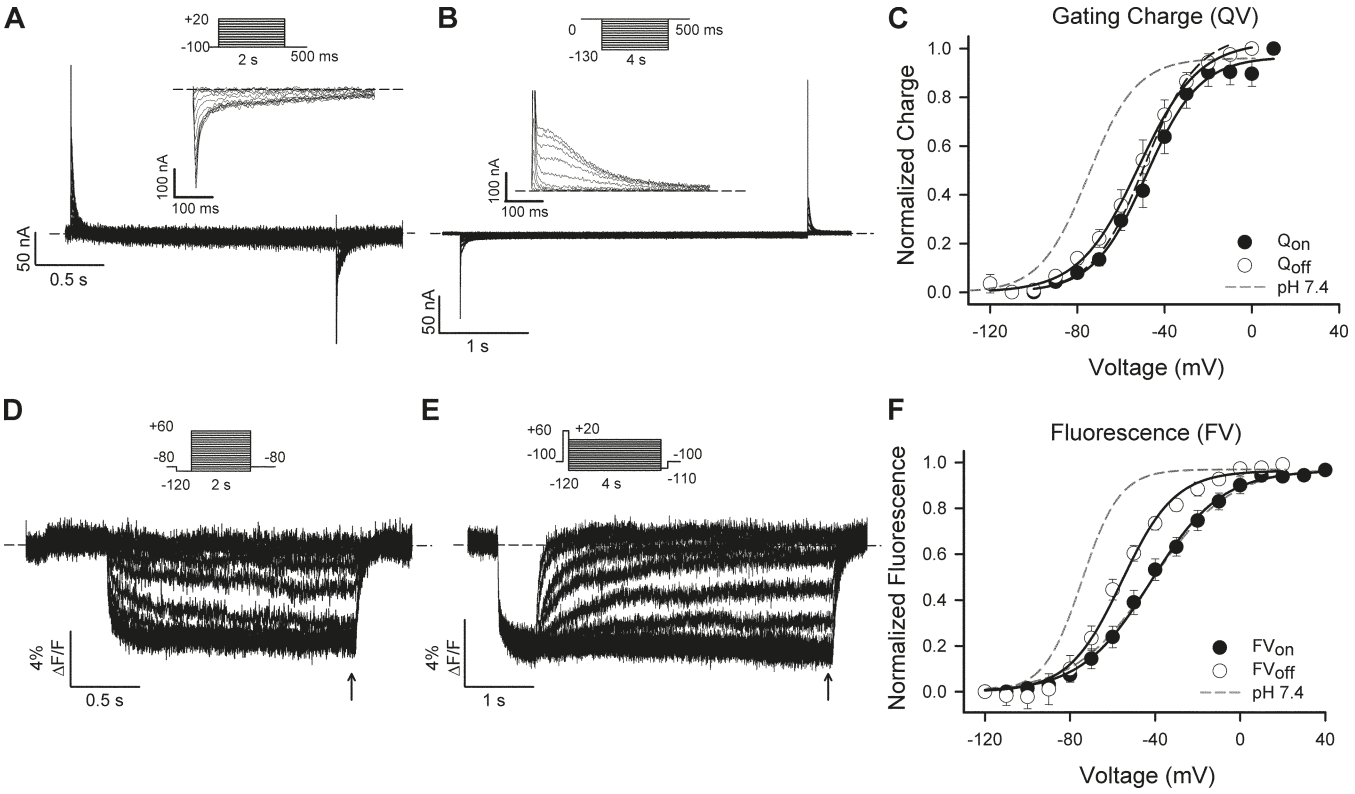

Figure 4. **Voltage sensor mode shift is reduced by acidic pH. (A and B)** Typical gating currents recorded at pH 6.5 in response to the voltage protocol shown (insets), as in Fig. 3. **(C)** Plot of the voltage dependence of Q_{on} and Q_{off}. Data were fitted with a Boltzmann function, which yielded $V_{1/2}$ values for Q_{on} and Q_{off} of −44.8 ± 5.0 mV (n = 8; not significantly different from pH 7.4, P > 0.5) and −51.8 ± 3.3 mV (n = 5; P < 0.0007 compared with pH 7.4), respectively. The mean gating current mode shift was reduced to −7.0 ± 6.0 mV. Dashed lines show pH 7.4 fits from Fig. 3 C for comparison. **(D and E)** Typical on-fluorescence (F_{on}; D) and off-fluorescence (F_{off}; E) reports from TMRM attached at L520C at pH 6.5 in response to the voltage protocols shown (insets). Arrows mark where fluorescence measurements were made. Dashed lines represent baseline. **(F)** Plot of the voltage dependence of F_{on} and F_{off}. F_{on}-V was constructed by measuring relative fluorescence change at the end of the 2-s depolarizing voltage step. F_{off}-V was constructed by measuring relative fluorescence change at the end of the 4-s repolarizing voltage step. Data were fitted with a Boltzmann function, which yielded $V_{1/2}$ values for F_{on} and F_{off} of −42.8 ± 3.7 mV (n = 5; not significantly different from pH 7.4, P > 0.5) and −57.2 ± 1.9 mV (n = 5; P < 0.001 compared with pH 7.4), respectively. The mean fluorescence mode shift was reduced to −14.4 ± 4.2 mV. Dashed lines show pH 7.4 fits from Fig. 3 F for comparison.

of −44.8 ± 5.0 mV (n = 8) and −51.8 ± 3.3 mV (n = 5) for Q_{on}-V and Q_{off}-V, respectively (Fig. 4 C), and of −42.8 ± 3.7 mV (n = 5) and −57.2 ± 1.9 mV (n = 5) for on- and off-fluorescence (Fig. 4 F). Thus, in both measures of voltage sensor gating, while the voltage dependence of activation gating was not greatly affected at pH 6.5 (see Table 3), the voltage dependence of voltage sensor return was robustly shifted to more depolarized potentials by +23.7 mV (gating charge, P < 0.05 compared with pH 7.4) and +18.9 mV (fluorescence, P < 0.05 compared with pH 7.4). This specific effect of protons on deactivation reduced the voltage sensor mode shift to −7.0 mV (gating charge) and −14.4 mV (fluorescence). These data show that acidic pH produces a robust reduction in voltage sensor mode shift by selectively reducing the energy required to return the voltage sensor to its resting configuration, consistent with a proton-induced destabilization of the relaxed configuration of the voltage sensor.

Destabilization of voltage sensor relaxation by protons is mediated by an extracellular acidic site, D509

Having established that external protons destabilize the activated relaxed state of the voltage sensor, we next investigated the interaction site of protons that mediates this effect. The activated position of the voltage sensor is thought to be stabilized by key electrostatic interactions between acidic residues D456 and D460 in S2 and D509 in S3, with positive residues in S4, such as R531 (Papazian et al., 1995; Liu et al., 2003; Piper et al., 2008). Previous studies have shown that the three acidic residues form a metal cation–binding pocket that coordinate cations, such as Ca^{2+}, Mg^{2+}, and Cd^{2+}, and is protonated by H^+; each of these ions depolarizes the voltage dependence of activation and accelerate the kinetics of deactivation (Ho et al., 1998; Anumonwo et al., 1999; Johnson et al., 1999a,b; Silverman et al., 2000; Fernandez et al., 2005; Abbruzzese et al., 2010; Kazmierczak et al., 2013; Shi et al., 2014). Neutralization of D509 in particular shifts the voltage dependence of activation to more depolarized potentials (Shi et al., 2014) and abolishes the proton-induced acceleration of deactivation (Liu et al., 2003). These observations suggest that D509 is an important site in stabilizing activated channel states (Shi et al., 2014), although this cannot be confirmed structurally since D509 is in a disordered or dynamic region of the latest cryo-EM hERG structures (Wang and MacKinnon, 2017). Despite the structural uncertainty, and driven by the available functional data, we investigated whether protonation of D509 destabilized the relaxed state of the voltage sensor. Although we were not able to re-

Table 3. **Charge–voltage and F-V relationship Boltzmann fit parameters for activation and deactivation**

	Q_{on}-V $V_{1/2}$ (mV)	*k*	Q_{off}-V $V_{1/2}$ (mV)	*k*	Mode shift $V_{1/2}$ (mV)
WT					
pH 7.4	−48.2 ± 0.5 (3)	12.2 ± 2.4	−75.5 ± 2.3 (4)	11.0 ± 0.7	−27.3 ± 2.4
pH 6.5	−44.8 ± 5.0 (8)	12.2 ± 1.0	−51.8 ± 3.3 (5)	13.7 ± 0.5	−7.0 ± 6.0
	F_{on}-V $V_{1/2}$ (mV)	*k*	F_{off}-V $V_{1/2}$ (mV)	*k*	Mode shift $V_{1/2}$ (mV)
L520C					
pH 7.4	−44.7 ± 1.0 (4)	21.3 ± 1.9	−76.1 ± 3.2 (5)	8.8 ± 0.5	−31.4 ± 3.4
pH 6.5	−42.8 ± 3.7 (5)	17.3 ± 0.8	−57.2 ± 1.9 (5)	15.5 ± 2.7	−14.4 ± 4.2
D509A/L520C					
pH 7.4	−40.9 ± 8.1 (4)	29.6 ± 2.9	−47.7 ± 3.7 (3)	25.8 ± 5.5	−5.6 ± 8.9
pH 6.5	−42.7 ± 3.5 (3)	27.2 ± 0.6	−49.6 ± 4.4 (3)	26.8 ± 1.3	−6.9 ± 5.6

Data are expressed as mean ± SEM, with the number of cells in parentheses.

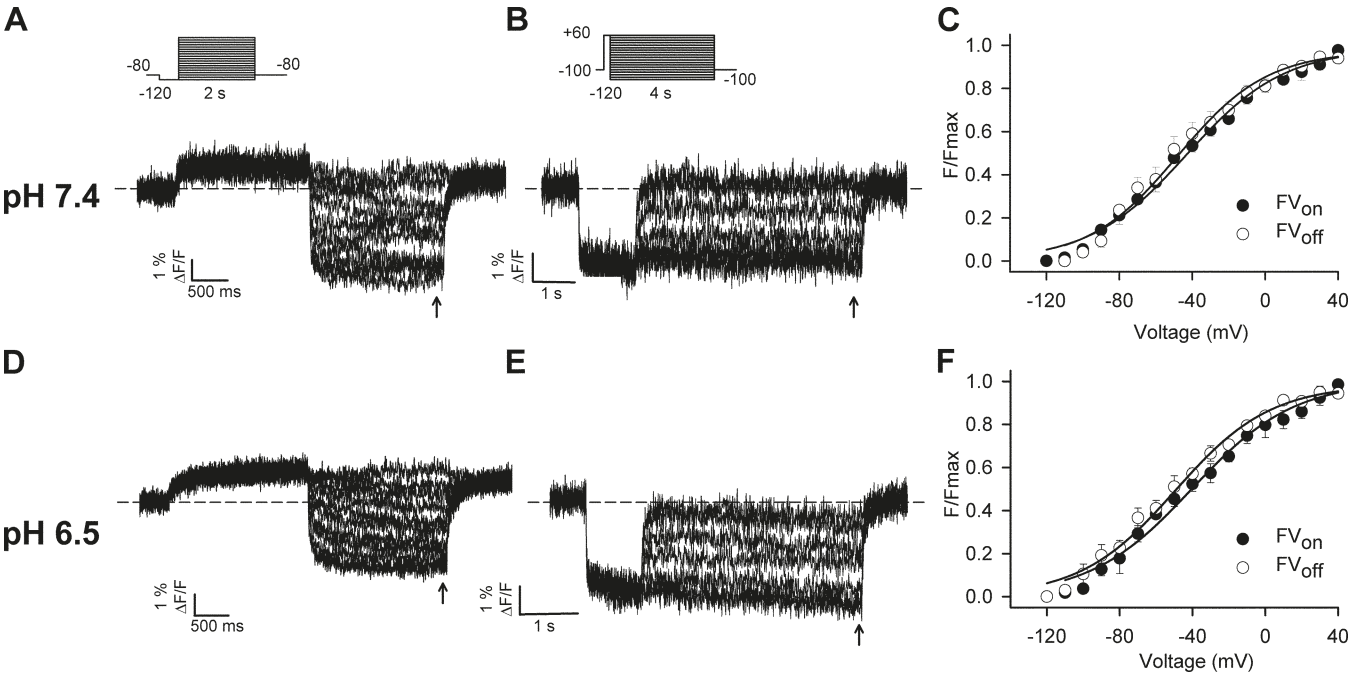

Figure 5. **Neutralization of D509 mimics the effect of protons on voltage sensor mode shift. (A, B, D, and E)** Typical on-fluorescence (A and D) and off-fluorescence (B and E) changes from TMRM attached at L520C in D509A mutant channels in response to the voltage protocols shown (insets) at pH 7.4 (A and B) and pH 6.5 (D and E). Arrows mark where fluorescence measurements were made. **(C and F)** Plots of the voltage dependence of F_{on} and F_{off} at pH 7.4 (C) and pH 6.5 (F). Data were fitted with a Boltzmann function, which yielded $V_{1/2}$ values for F_{on} and F_{off} of −52.2 ± 8.1 mV (n = 4) and −57.8 ± 3.7 (n = 3), respectively, at pH 7.4. The corresponding values at pH 6.5 were −42.7 mV ± 3.5 (n = 3) and −49.6 mV ± 4.4 (n = 4), respectively. The mean voltage sensor mode shift was −5.6 ± 8.9 mV at pH 7.4 and −6.9 mV ± 2.1 at pH 6.5. Dashed lines represent baseline.

solve gating current recordings from D509A mutant channels, we recorded resolvable fluorescence reports of voltage sensor movement using TMRM labeling at L520C in D509A mutant channels. Fig. 5 (A and B) shows typical fluorescence reports of voltage sensor movement in D509A channels during the voltage protocols shown, from which on-fluorescence and off-fluorescence voltage relationships were constructed (Fig. 5 C). Fig. 5 (D and E) shows fluorescence records using the same voltage protocols, but with the external solution titrated to pH 6.5. It is clear that the characteristic separation of the voltage dependencies of voltage sensor activation and deactivation that result from relaxation is largely abolished by neutralization of D509 and that acidic pH has no additional effect on voltage sensor gating in the D509A mutant channel. The reduced separation was largely caused by a right shift of the voltage dependence of deactivation (F_{off}) in D509A mutant channels (+18.3 mV), with little effect on the F_{on} relationship (Table 3). Thus, neutralization of D509 mimicked the effect of pH 6.5, largely abolishing the mode shift due to voltage sensor relaxation. These data indicate that D509 is a critical site involved in stabilization of the relaxed state.

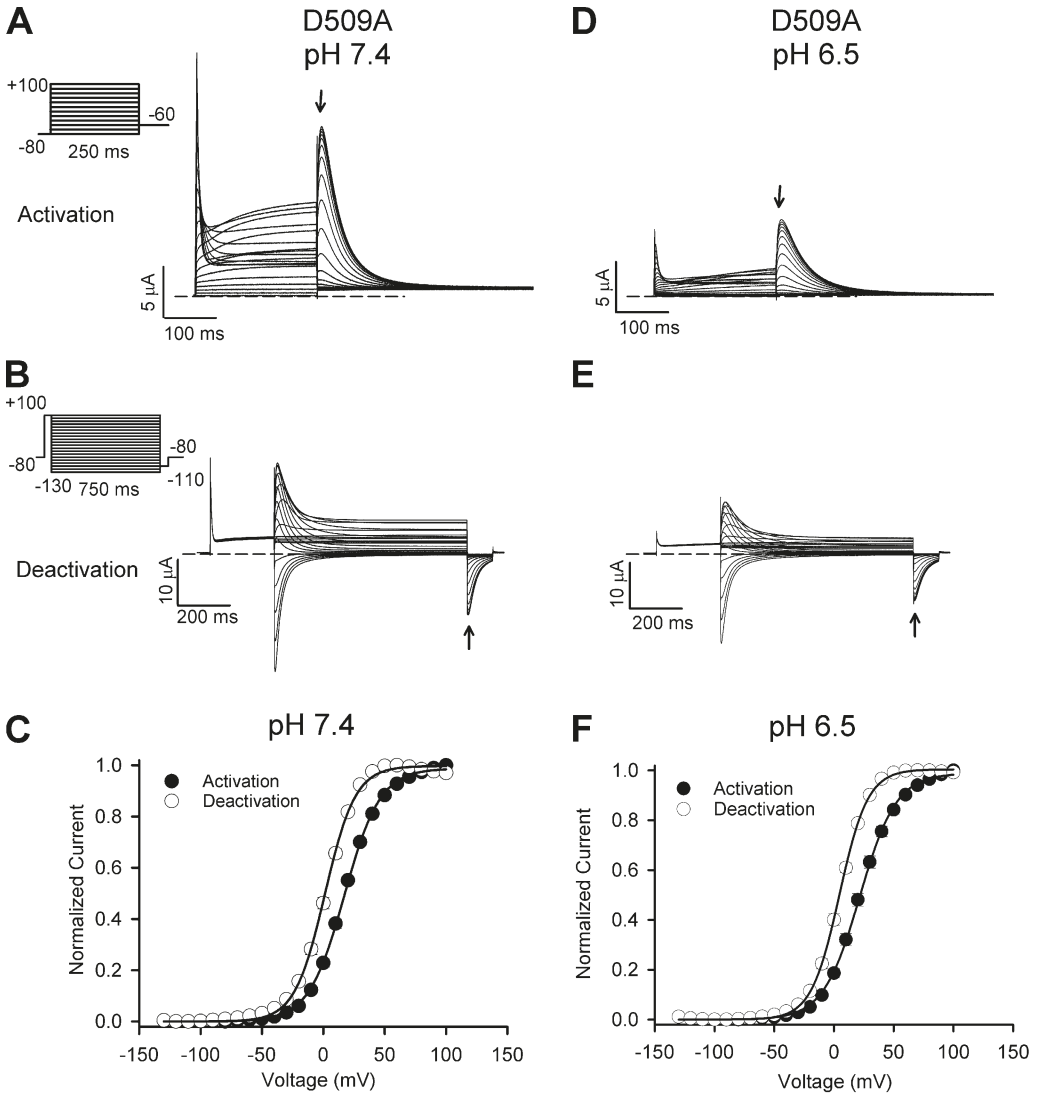

Figure 6. **Mode shift is greatly diminished and is pH independent in D509A mutant channels. (A and D)** Typical ionic current recordings from D509A mutant channels at pH 7.4 (A) or pH 6.5 (D) in response to the voltage protocols shown (insets) designed to measure the voltage dependence of activation. The membrane was held at −80 mV before 250-ms steps were applied up to +100 mV (in 10-mV increments), followed by a repolarizing step to −60 mV. Arrows mark where current measurements were made. **(B and E)** Typical ionic current recordings of D509A channel deactivation at pH 7.4 (B) or pH 6.5 (E). The membrane was held at −80 mV before a 250-ms depolarizing step to +100 mV, followed by 750-ms repolarizing steps down to −130 mV (in 10-mV increments). **(C and F)** Plots of the voltage dependence of activation and deactivation at pH 7.4 (C) and pH 6.5 (F). Data were fitted with a Boltzmann function, which yielded $V_{1/2}$ values for activation and deactivation of +17.1 ± 0.8 mV (n = 5) and +1.6 ± 1.1 mV (n = 5), respectively, at pH 7.4. The corresponding values at pH 6.5 were +21.6 ± 1.5 mV (n = 5) and +4.8 ± 1.2 mV (n = 5), respectively. The mean mode shift was −15.5 ± 0.1 mV at pH 7.4 and −16.8 mV ± 0.6 at pH 6.5 ($P > 0.3$; not significantly different, Student's t test; see Table 1). Dashed lines represent baseline.

If destabilization of the relaxed state of the voltage sensor results in an acceleration of deactivation kinetics as the data in Figs. 1 and 2 suggest, measurement of D509A ionic currents should exhibit fast deactivation. Fig. 6 shows that this is indeed the case. Typical families of D509A ionic currents recorded at pH 7.4 or pH 6.5 using the voltage protocol shown demonstrate accelerated deactivation kinetics in D509A mutant channels, which were resistant to further acceleration by switching to acidic pH. This is consistent with the conclusion that slow deactivation gating in hERG channels arises from stabilization of the relaxed state of the voltage sensor. These findings highlight the physiological significance of entry of the hERG voltage sensor into the stabilized state, that is, destabilization of the relaxed state leads to accelerated deactivation and loss of mode shift behavior.

Discussion

Recent attention has been given to mode shift behavior in hERG channels, in part because the pronounced separation of activation and deactivation gating energetics appears to occur in response to physiologically relevant depolarization durations (Fig. 1), but also because stabilization of activated states that slows deactivation gating may provide therapeutic strategies for enhancing channel availability. We have previously shown that mode shift behavior in hERG channels is caused by both slow activation and, more impor-

tantly, slow deactivation gating (Thouta et al., 2017). It is important, therefore, to better understand the mechanism by which slow deactivation gating arises. Several studies have shown that prolonged depolarizations slow hERG voltage sensor return and pore closure (Tan et al., 2012; Goodchild et al., 2015; Thouta et al., 2017), suggesting a role for relaxation in the control of deactivation gating. Consistent with this, hERG channels display robust voltage sensor domain relaxation, such that the voltage dependence of sensor return is left shifted from that of pore gate closure (Thouta et al., 2017). This suggests that the energy barrier for exiting the relaxed state is rate limiting for deactivation. The observation that partial charge return is sufficient to induce pore gate closure (Thouta et al., 2017) is consistent with observations in *Shaker* channels, where return of a single voltage sensor is sufficient to close the channel pore (Gagnon and Bezanilla, 2009). Together, the data allow for the generation of a hypothesis that stabilization of activated S4 sensors by relaxation limits hERG pore closure.

The effects of acidic pH support a correlation between mode shift and deactivation kinetics

In the present study, we have used acidic pH to explore this hypothesis that relaxation limits deactivation, and in doing so, also attempt to understand the mechanistic basis for the pH-induced acceleration of hERG channel gating, which has been the subject of significant previous interest (Bérubé et al., 1999; Jiang et al., 1999; Terai et al., 2000; Bett and Rasmusson, 2003; Liu et al., 2003; Du et al., 2010; Shi et al., 2014). We show that acidic external pH reduces the mode shift behavior measured from ionic activation and deactivation gating (Fig. 2) and that this is largely due to a specific effect on the voltage dependence of deactivation gating. These data show that external protons shift the voltage dependence of deactivation to the right, indicating a reduction in the energetic stability of the activated state and a relative increase in the stability of the closed state of the pore. Interestingly, the pH dependence of this effect was very similar to that describing the acceleration of deactivation kinetics (Fig. 2, compare C with F), which has been described previously (Bett and Rasmusson, 2003). Such a similarity is consistent with the idea that the kinetics of deactivation gating correlate with the extent of mode shift behavior measured from ionic currents (e.g., Fig. 1).

External protons destabilize the relaxed voltage sensor

To understand the pH-induced acceleration of deactivation gating and reduced energetic stability of the open state, we recorded voltage sensor gating using combined approaches of charge measurement and fluorimetric reports of gating-associated conformational changes sensed at the outer end of S4. Congruence of measurements of fluorescence reports with those of gating charge address uncertainty concerning the interpretation of fluorimetric reports from the hERG voltage sensor. Previous reports of fluorescence changes from TMRM attached at L520C at the top of the voltage sensor displayed a voltage dependence more similar to that of pore opening than of gating charge movement (Es-Salah-Lamoureux et al., 2010; Van Slyke et al., 2010), suggesting that the reports may track pore gating maneuvers rather than voltage sensing. However, we find close agreement of the voltage dependence of charge movement and fluorescence signals when a prepulse to −120 mV was used to measure the latter (Table 3 and Fig. S1). These data show a fluorescence dequenching upon hyperpolarization from −80 mV, indicating that more hyperpolarized voltages are required to return the voltage sensor to its resting position. Using a prepulse to −120 mV allowed capture of the full F-V, which closely aligned with that of the isochronal charge–voltage relationship. These data demonstrate consistency in the reports of voltage sensor movement from measurement of charge movement and fluorescence changes.

Both approaches reported a profound depolarizing shift in the voltage dependence of voltage sensor return at pH 6.5 without altering voltage sensor activation (Figs. 3 and 4). This indicates that in the pathophysiologically relevant pH range tested, external protons have little effect on the transitions of the voltage sensor into the activated state but specifically affect interactions that stabilize the voltage sensor in its activated state. Stabilization of the activated voltage sensor following activation has been demonstrated in numerous channels and voltage sensor–like proteins and has been attributed to a process termed relaxation (Brum et al., 1987; Elinder et al., 2006; Villalba-Galea et al., 2008; Haddad and Blunck, 2011; Labro et al., 2012; Priest et al., 2013; Villalba-Galea, 2014). Relaxation appears to be an intrinsic property of the voltage sensing unit and involves interactions that stabilize the extruded position of the voltage sensor (Villalba-Galea et al., 2008; Haddad and Blunck, 2011). Such stabilization increases the energetic cost of voltage sensor return, shifting the voltage dependence to more hyperpolarized potentials and separating it from that of voltage sensor activation. Our findings suggest that external protons destabilize the relaxed state of the voltage sensor, catalyzing voltage sensor return and thus pore closure.

To test this, we constructed a kinetic model using IonChannelLab (Santiago-Castillo et al., 2010) to describe voltage sensor gating transitions between resting, activated, and relaxed states (Fig. 7 A). The Markov state model in Fig. 7 A is a simplified form of a previous model used to describe hERG gating (Piper et al., 2003), and it considers transitions of the voltage sensor domain alone in an attempt to model the voltage sensor behavior observed in our study. As in the original model (Piper et al., 2003), the scheme in Fig. 7 A includes two independent conformational changes in each subunit of the tetramer (S0–S1 and S1–S2) that are voltage dependent followed by a concerted transition to the activated state (A). Forward rates were calculated as $\alpha = \alpha_o \times \exp(z\alpha \times VF/RT)$, and reverse rates were calculated as $\beta = \beta_o \times \exp(z\beta \times VF/RT)$. As described previously (Piper et al., 2003), it was necessary to include a positive cooperativity factor in the rates to recapitulate the fast and slow phases of gating current observed experimentally (see also Table 4). The scheme in Fig. 7 A also includes a voltage sensor transition into the relaxed state with the intent to simulate mode shift behavior of the voltage sensor. The term $z\alpha$ in the forward rate was set to zero, consistent with previous reports that entry into the relaxed state is voltage independent (Villalba-Galea et al., 2008). Thus, transition into the relaxed state is modeled as being time dependent with a forward rate constrained by previous measurements of the kinetics of entry of the voltage sensor into the relaxed state (Thouta et al., 2017). The backward rate for the transition out of the relaxed state is termed de-relaxation, consistent with a previous description in *Shaker* channels (Priest et al., 2013).

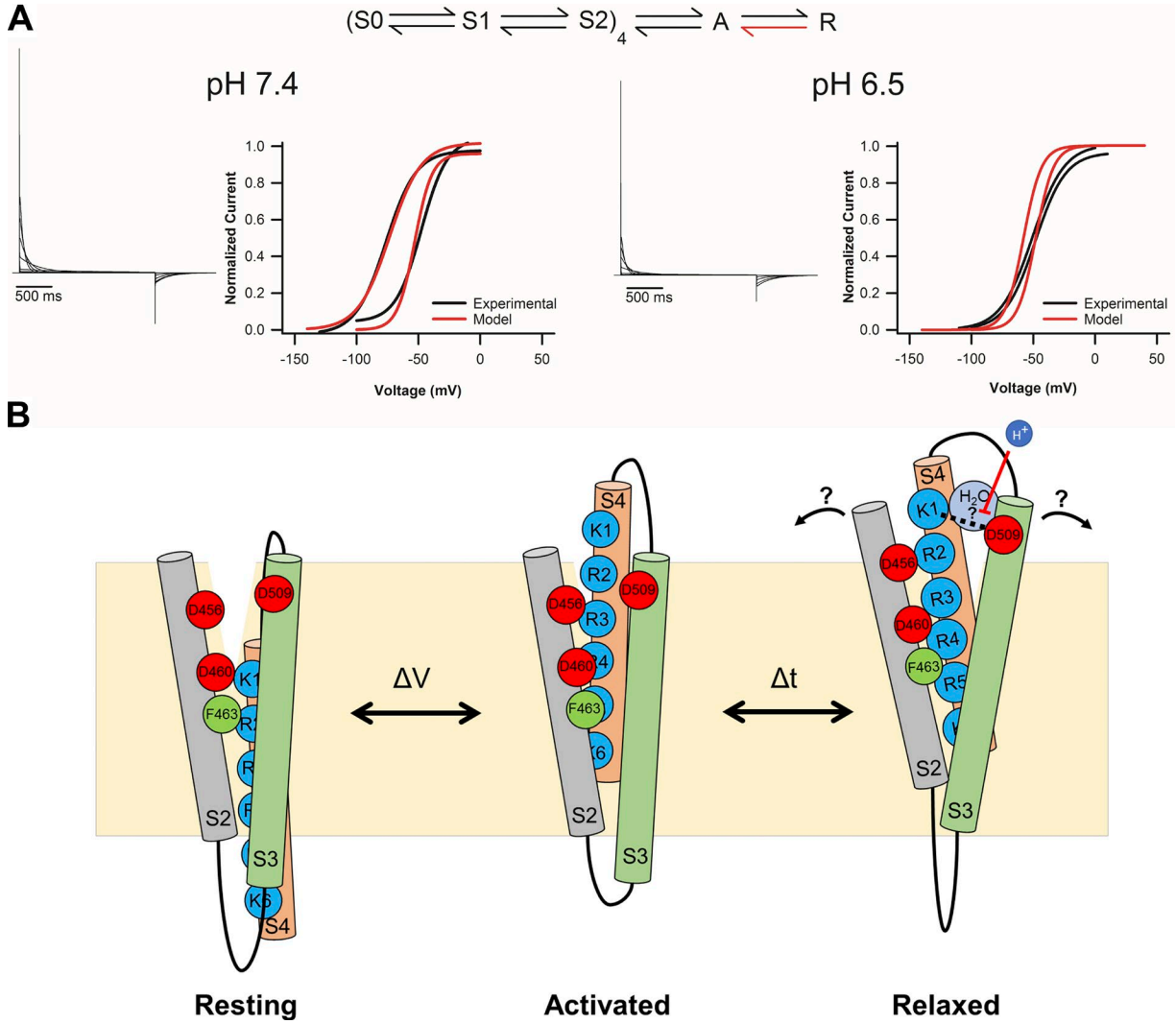

Figure 7. **Model of hERG voltage sensor relaxation. (A)** Markov gating scheme used to model hERG voltage sensor gating at pH 7.4 and pH 6.5 (top). Details are provided in the text, and transition rates are described in Table 4. The transition highlighted red represents that which was modified to simulate voltage sensor behavior at pH 6.5. Simulated on-gating currents using the model along with predicted on- and off-gating currents are shown for pH 7.4 (lower left) and pH 6.5 (lower right). Boltzmann fits yielded $V_{1/2}$ values of −52.8 mV and −73.0 mV for Q_{on}-V and Q_{off}-V, respectively, at pH 7.4 (mode shift = −20.2 mV). At pH 6.5, equivalent values were −47.9 mV and −54.7 mV (mode shift = −6.8 mV). The salient features of gating currents at pH 6.5 could be modeled by accelerating the rate of de-relaxation. **(B)** Cartoon representation of proposed reconfigurations of S2, S3, and S4 voltage sensor transmembrane domains in the resting, activated, and relaxed state. K1 and K6 refer to K525 and K538, respectively. R1–R5 describe R528–R537. Putative reconfigurations associated with entry into the relaxed state are shown, which may involve stabilizing interactions of D509 with outer S4 positive charges either directly or via a water molecule network. Neutralization of D509 or external protonation is predicted to destabilize these interactions and consequently the relaxed state.

Fig. 7 A shows simulated on-gating currents produced by the model. These simulations demonstrate that the model is capable of recapitulating the main features of hERG on-gating currents recorded experimentally, including the prominent fast and slow phases of charge movement, as well as both the voltage dependence of on-gating charge movement and the separation of the voltage dependence of the off-gating current that we describe as mode shift behavior. To model voltage sensor gating behavior at pH 6.5, we simply adjusted the backward rate for the relaxation transition, such that de-relaxation was accelerated (Table 4). Manipulating this rate in this way reproduced the effects of acidic pH on voltage sensor gating that we observed experimentally. There was little effect on on-gating behavior, but off-gating was accelerated, and there was a pronounced right shift of the voltage dependence of off-gating charge movement that resulted in reduction of mode shift behavior. While this may not be a unique solution and the slope factors of the model output are somewhat steeper, the model is able to emulate the main features of observed voltage sensor behavior and supports our conclusion that external protons destabilize the relaxed state of the voltage sensor, leading to accelerated charge return.

Site and mechanism of action of external protons

Numerous previous studies have attempted to define the site and mechanism of action of protons that determines the pH-induced acceleration of deactivation gating in hERG channels (Bérubé et al., 1999; Bett and Rasmusson, 2003; Liu et al., 2003; Zhang et al., 2005; Piper et al., 2008). We demonstrate in Figs. 3 and 4

Table 4. **Rates and factors for the Markov model**

Transition	α_o (s^{-1})	$z\alpha_o$(s^{-1})	β_o (s^{-1})	$z\beta_o$ (s^{-1})	*c*
S0–S1	1,000	0.2	1,500	−0.04	1
S1–S2	134	0.02	280	−0.05	1.5
S2–A	2,000	2	0.006	−1.7	
A–R					
pH 7.4	0.5	0	0.001	0	
pH 6.5			10	0	

Parameters for pH 6.5 were the same as those for pH 7.4, unless otherwise indicated. Forward rates were calculated as $\alpha = \alpha_o * \exp(z\alpha * VF/RT)$, and reverse rates were calculated as $\beta = \beta_o * \exp(z\beta * VF/RT)$. *c* reflects the cooperativity factor applied to the independent transitions. It was necessary to modify forward and backward rates between S2 and A states from those reported previously (Piper et al., 2003) to reproduce gating current properties during the longer durations used in the present study.

that protons specifically reduce the energetics of voltage sensor return, and our kinetic simulations (Fig. 7 A) suggest that the relaxed state of the voltage sensor is destabilized. Since protons are applied externally, these findings imply that the destabilization of the relaxed state is mediated by an external site that is associated with the voltage-sensing unit. Previously, we and others have shown that more extreme acidification than used in the present study right-shifts the voltage dependence of voltage sensor activation via protonation of acidic residues D456, D460, and D509 in S2 and S3 (Kazmierczak et al., 2013; Shi et al., 2014). Cations, such as Ca^{2+}, Cd^{2+}, Mg^{2+}, and Zn^{2+}, also coordinate with these sites, which form a discrete binding pocket (Ho et al., 1998; Anumonwo et al., 1999; Johnson et al., 2001; Fernandez et al., 2005; Abbruzzese et al., 2010; Kazmierczak et al., 2013; Shi et al., 2014). Of the acidic charges forming the S2–S3-binding pocket, D509 was shown to have the greatest influence on the ability of protons to shift the voltage dependence of hERG channel activation gating (Shi et al., 2014), and therefore, we focused attention on this site in the present study. The data in Fig. 5 suggest that protonation at D509 modifies the stability of the relaxed state of the voltage sensor, since neutralization of this site largely abolished mode shift of the voltage sensor by shifting the voltage dependence of voltage sensor return. This destabilization of the relaxed voltage sensor is associated with accelerated closure of the pore gate, as evidenced by the rapid ionic current deactivation (Fig. 6), consistent with our conclusion that the stability of the relaxed voltage sensor contributes to hERG deactivation kinetics. We interpret these findings to suggest that titration of the native charge at D509 by external protons destabilizes the relaxed state of the voltage sensor, decreasing the energy barrier for deactivation and accelerating deactivation kinetics. Fig. 7 B shows a cartoon representation of how this might occur. This model, which depicts the hERG S2, S3, and S4 helices with putative interactions associated with transitions between resting, activated, and relaxed states, is based on a number of findings. The external acidic residues in S2 and S3 (D456, D460, and D509) have previously been reported to be involved in stabilizing ionic interactions with S4 gating charges (Papazian et al., 1995; Liu et al., 2003; Zhang et al., 2005; Piper et al., 2008). For example, double-mutant cyclic analysis has shown energetic coupling between R531 and D456, D460, and D509, as well as D411 and D466, through a cooperative electrostatic interaction mechanism (Piper et al., 2008), and accessibility studies have revealed that D460 and D509 increase the stability of the activated state (Liu et al., 2003). For this reason, the activated voltage-sensing unit is depicted with R531 (R3) in close proximity with D456, D460, and D509, which themselves are closely positioned to form the cation-binding pocket, as shown in previous functional studies (Kazmierczak et al., 2013; Shi et al., 2014). In the model, K525 (K1) moves upon activation from a lipid-embedded location to become exposed to the extracellular environment, consistent with accessibility studies (Elliott et al., 2009), and is in close proximity to the gating charge transfer center residue, F463, with which it has been shown to form functional interactions that stabilize the resting state (Cheng et al., 2013). Activation of the voltage-sensing unit presumably involves S4 charges shuttling through the F463 gating charge transfer center, as has been suggested in Shaker (Tao et al., 2010), with R537 (R5) and K538 (K6) aligning closely with F463 in the activated state, consistent with evidence suggesting functional interactions between the innermost basic charges and the phenylalanine that stabilize the activated state (Cheng et al., 2013). Importantly, D509 occupies a position that is readily accessible to extracellular aqueous solvent, as shown previously (Liu et al., 2003). The model in Fig. 7 B also includes possible time-dependent, voltage-independent transitions associated with stabilization of the voltage-sensing unit into the relaxed state. Reconfigurations during this gating step are likely to be subtle given that they are not associated with charge translocation across the membrane and are not readily observable as environmental change in the report from fluorophores attached at the top of S4. We propose that relaxation in hERG channels could involve a widening of the cleft between the outer ends of the S2, S3, and S4 helices that either stabilizes interactions between D509 and S4 basic charges, such as R528 (R2), or enables D509 to form H-bonds or electrostatic interactions with water molecules within the water-filled crevice. In the latter case, this could establish a network of interactions that then bridge the acidic residue with positive residues in S4, similar to that described for external acidic charges in the Hv1 proton channel (Ramsey et al., 2010; De La Rosa et al., 2018). This possibility is consistent with the observation that the presence of water molecules in an aqueous extracellular crevice at the outer end of S4 influences the stability of the activated voltage sensor via interactions with S4 positive charges (Bezanilla, 2000; Swartz, 2008; Ramsey et al., 2010; Islas, 2016). In the model, stabilization of these salt bridge interactions or water molecule networks contributes to the stability of the activated state of the hERG voltage sensor and precipitates entry of the sensor into the relaxed state. In this scenario, destabilization of these interactions by neutralization of D509, or by titration of the charge with external acidification, would disrupt this extracellular electrostatic network to destabilize the activated voltage sensor, reducing the energetic barrier for its return to the resting state. Since only fractional charge return, perhaps a single S4 in the tetramer, appears to be required to close the pore gate (Thouta et al., 2017), similar to

that suggested in Shaker channels (Gagnon and Bezanilla, 2009), this would result in accelerated channel deactivation. This model thus establishes a working hypothesis of the mechanism underlying relaxation of the voltage sensor in hERG channels and how voltage sensor gating is influenced by external protons.

Refinement of high-resolution structures of the hERG voltage sensor would contribute to confirming this working model, since the current cryo-EM structure (Wang and MacKinnon, 2017) possesses a disordered upper S3 helical structure that introduces uncertainty as to the position of D509. This could indicate that the upper S3 helix is highly dynamic, thus reducing the resolution, or alternatively that the resolved S3 structure is in some way perturbed (e.g., has become partially unwound due to denaturing purification conditions). Further structural refinement may also aid our description of D509 as a proton sensor. For example, while the *pKa* for the side chain of D509 in free solution is 3.71, it is conceivable that the local environment may modify the *pKa* of D509, allowing protonation of the side chain at pH 6.5. Although extracellular histidine residues are the most likely candidates as proton sensors (*pKa* = 6.0), a previous study showed that mutation of the five histidine residues that are accessible to the extracellular environment to glutamine did not reduce the proton-induced acceleration of deactivation (Van Slyke et al., 2012). We used ROSETTA to predict the *pKa* of the D509 side chain based on the cryo-EM hERG structure (Wang and MacKinnon, 2017) to evaluate whether the *pKa* might be influenced by the surrounding environment. However, this approach predicted values equivalent to an aspartate in free solution and is likely limited by the fact that D509 is located in a highly dynamic or less well-ordered region in the available structures. Further structural information that includes, for example, D509 contributing to a cation-binding pocket constructed by D456, D460, and D509, as has been shown previously in functional studies (Fernandez et al., 2005; Kazmierczak et al., 2013), may influence the predicted *pKa* of the aspartate due to tighter packing of the residue than is evident in the available cryo-EM structure. Such information could provide valuable insight to the role of D509 in stabilization of voltage sensor relaxation in hERG channels.

The stability of the relaxed state modulates deactivation kinetics in hERG channels

It is interesting to note that the *pKa* for the effect of external protons on deactivation gating (pH 7.0) that is mediated through D509 (Fig. 2) is different from that which we reported previously for the acidic pH–induced shift in the voltage dependence of activation (pH 5.4) that is mediated by the same site (Shi et al., 2014). That D509 mediates both entry into the activated state and the stability of the relaxed state is, however, consistent with our conclusion that titration of D509 influences charge–charge interactions within the voltage-sensing unit that are important for S4 gating. The differing pH dependence suggests a greater sensitivity of the relaxed state to the charge on D509. This may be because the pH sensitivity of the voltage dependence of activation involves a complex interplay and coordination between D456, D460, and D509 in the cation-binding pocket as channels transition into the open state (Piper et al., 2008). Therefore, a higher degree of protonation at multiple sites may be required to alter the activation transition pathway (*pKa* = 5.4). This would support the observation that D509, together with coordination of D456 and D460, is involved in the activation gating of hERG channels (Shi et al., 2014). In contrast, protonation of D509 alone was sufficient to destabilize the relaxed conformation of the voltage sensor. One explanation for this may be that relaxation occurs from the activated state when the stabilizing ionic interactions within the voltage-sensing unit are exposed to the extracellular milieu and may be more readily protonated. Alternatively, it may be that the interactions involving D509 are important when the voltage sensor is in the fully activated and/or relaxed state and that D456 and D460 are important during the intermediate transitions along the activation pathway.

In summary, we propose that return of the voltage sensor from the relaxed state, i.e., de-relaxation, acts functionally as a "master switch" (a previously used term; Liu et al., 2003) that regulates deactivation gating. In this way, de-relaxation is the limiting step that allows return of the fraction of charge required to close the pore gate. We propose that mutations within the voltage-sensing unit may accelerate deactivation gating by modifying the stability of the relaxed state of the voltage sensor, disrupting the extracellular water molecule network or salt bridge formations between S4 charges and their countercharges within the voltage-sensing unit, or modifying the electric field within which these interactions take place.

Acknowledgments

This research was supported by a Heart and Stroke Foundation of Canada and Yukon Grant-In-Aid and a Natural Sciences and Engineering Research Council of Canada Discovery Grant (T.W. Claydon).

The authors declare no competing financial interests.

Author contributions: Y.P. Shi, S. Thouta, Y.M. Cheng, and T.W. Claydon conceived the project and wrote the article, and Y.P. Shi and S. Thouta performed experiments and data analysis.

Sharona E. Gordon served as editor.

Submitted: 4 June 2018
Revised: 23 August 2018
Accepted: 7 November 2018

References

Abbruzzese, J., F.B. Sachse, M. Tristani-Firouzi, and M.C. Sanguinetti. 2010. Modification of hERG1 channel gating by Cd^{2+}. *J. Gen. Physiol.* 136:203–224. https://doi.org/10.1085/jgp.201010450

Adaixo, R., C.A. Harley, A.F. Castro-Rodrigues, and J.H. Morais-Cabral. 2013. Structural properties of PAS domains from the KCNH potassium channels. *PLoS One.* 8:e59265. https://doi.org/10.1371/journal.pone.0059265

Al-Owais, M., K. Bracey, and D. Wray. 2009. Role of intracellular domains in the function of the herg potassium channel. *Eur. Biophys. J.* 38:569–576. https://doi.org/10.1007/s00249-009-0408-2

Anumonwo, J.M.B., J. Horta, M. Delmar, S.M. Taffet, and J. Jalife. 1999. Proton and zinc effects on HERG currents. *Biophys. J.* 77:282–298. https://doi.org/10.1016/S0006-3495(99)76889-X

Bérubé, J., M. Chahine, and P. Daleau. 1999. Modulation of HERG potassium channel properties by external pH. *Pflugers Arch.* 438:419–422. https://doi.org/10.1007/s004240050930

Bett, G.C.L., and R.L. Rasmusson. 2003. Functionally-distinct proton-binding in HERG suggests the presence of two binding sites. *Cell Biochem. Biophys.* 39:183–193. https://doi.org/10.1385/CBB:39:3:183

Bezanilla, F. 2000. The voltage sensor in voltage-dependent ion channels. *Physiol. Rev.* 80:555–592. https://doi.org/10.1152/physrev.2000.80.2.555

Brelidze, T.I., E.C. Gianulis, F. DiMaio, M.C. Trudeau, and W.N. Zagotta. 2013. Structure of the C-terminal region of an ERG channel and functional implications. *Proc. Natl. Acad. Sci. USA.* 110:11648–11653. https://doi.org/10.1073/pnas.1306887110

Bruening-Wright, A., and H.P. Larsson. 2007. Slow conformational changes of the voltage sensor during the mode shift in hyperpolarization-activated cyclic-nucleotide-gated channels. *J. Neurosci.* 27:270–278. https://doi.org/10.1523/JNEUROSCI.3801-06.2007

Brum, G., E. Stefani, and E. Rios. 1987. Simultaneous measurements of Ca^{2+} currents and intracellular Ca^{2+} concentrations in single skeletal muscle fibers of the frog. *Can. J. Physiol. Pharmacol.* 65:681–685. https://doi.org/10.1139/y87-112

Brum, G., E. Ríos, and E. Stéfani. 1988. Effects of extracellular calcium on calcium movements of excitation-contraction coupling in frog skeletal muscle fibres. *J. Physiol.* 398:441–473. https://doi.org/10.1113/jphysiol.1988.sp017052

Chen, J., A. Zou, I. Splawski, M.T. Keating, and M.C. Sanguinetti. 1999. Long QT syndrome-associated mutations in the Per-Arnt-Sim (PAS) domain of HERG potassium channels accelerate channel deactivation. *J. Biol. Chem.* 274:10113–10118. https://doi.org/10.1074/jbc.274.15.10113

Cheng, Y.M., C.M. Hull, C.M. Niven, J. Qi, C.R. Allard, and T.W. Claydon. 2013. Functional interactions of voltage sensor charges with an S2 hydrophobic plug in hERG channels. *J. Gen. Physiol.* 142:289–303. https://doi.org/10.1085/jgp.201310992

Curran, M.E., I. Splawski, K.W. Timothy, G.M. Vincent, E.D. Green, and M.T. Keating. 1995. A molecular basis for cardiac arrhythmia: HERG mutations cause long QT syndrome. *Cell.* 80:795–803. https://doi.org/10.1016/0092-8674(95)90358-5

de la Peña, P., A. Machín, J. Fernández-Trillo, P. Domínguez, and F. Barros. 2013. Mapping of interactions between the N- and C-termini and the channel core in HERG K^+ channels. *Biochem. J.* 451:463–474. https://doi.org/10.1042/BJ20121717

de la Peña, P., A. Machín, J. Fernández-Trillo, P. Domínguez, and F. Barros. 2015. Interactions between the N-terminal tail and the gating machinery of hERG K^+ channels both in closed and open/inactive states. *Pflugers Arch.* 467:1747–1756. https://doi.org/10.1007/s00424-014-1612-1

de la Peña, P., P. Domínguez, and F. Barros. 2018. Gating mechanism of Kv11.1 (hERG) K^+ channels without covalent connection between voltage sensor and pore domains. *Pflugers Arch.* 470:517–536. https://doi.org/10.1007/s00424-017-2093-9

De La Rosa, V., A.L. Bennett, and I.S. Ramsey. 2018. Coupling between an electrostatic network and the Zn^{2+} binding site modulates Hv1 activation. *J. Gen. Physiol.* 150:863–881. https://doi.org/10.1085/jgp.201711822

Du, C.Y., I. Adeniran, H. Cheng, Y.H. Zhang, A. El Harchi, M.J. McPate, H. Zhang, C.H. Orchard, and J.C. Hancox. 2010. Acidosis impairs the protective role of hERG $K(^+)$ channels against premature stimulation. *J. Cardiovasc. Electrophysiol.* 21:1160–1169. https://doi.org/10.1111/j.1540-8167.2010.01772.x

Elinder, F., R. Männikkö, S. Pandey, and H.P. Larsson. 2006. Mode shifts in the voltage gating of the mouse and human HCN2 and HCN4 channels. *J. Physiol.* 575:417–431. https://doi.org/10.1113/jphysiol.2006.110437

Elliott, D.J.S., N.Y. Dondas, T.S. Munsey, and A. Sivaprasadarao. 2009. Movement of the S4 segment in the hERG potassium channel during membrane depolarization. *Mol. Membr. Biol.* 26:435–447. https://doi.org/10.3109/09687680903321081

Es-Salah-Lamoureux, Z., R. Fougere, P.Y. Xiong, G.A. Robertson, and D. Fedida. 2010. Fluorescence-tracking of activation gating in human ERG channels reveals rapid S4 movement and slow pore opening. *PLoS One.* 5:e10876. https://doi.org/10.1371/journal.pone.0010876

Fernandez, D., A. Ghanta, K.I. Kinard, and M.C. Sanguinetti. 2005. Molecular mapping of a site for Cd2+-induced modification of human ether-à-go-go-related gene (hERG) channel activation. *J. Physiol.* 567:737–755. https://doi.org/10.1113/jphysiol.2005.089094

Fernández-Trillo, J., F. Barros, A. Machín, L. Carretero, P. Domínguez, and P. de la Peña. 2011. Molecular determinants of interactions between the N-terminal domain and the transmembrane core that modulate hERG K+ channel gating. *PLoS One.* 6:e24674. https://doi.org/10.1371/journal.pone.0024674

Ferrer, T., J. Rupp, D.R. Piper, and M. Tristani-Firouzi. 2006. The S4-S5 linker directly couples voltage sensor movement to the activation gate in the human ether-a'-go-go-related gene (hERG) K^+ channel. *J. Biol. Chem.* 281:12858–12864. https://doi.org/10.1074/jbc.M513518200

Gagnon, D.G., and F. Bezanilla. 2009. A single charged voltage sensor is capable of gating the *Shaker* K^+ channel. *J. Gen. Physiol.* 133:467–483. https://doi.org/10.1085/jgp.200810082

Goodchild, S.J., and D. Fedida. 2014. Gating charge movement precedes ionic current activation in hERG channels. *Channels (Austin).* 8:84–89. https://doi.org/10.4161/chan.26775

Goodchild, S.J., L.C. Macdonald, and D. Fedida. 2015. Sequence of gating charge movement and pore gating in HERG activation and deactivation pathways. *Biophys. J.* 108:1435–1447. https://doi.org/10.1016/j.bpj.2015.02.014

Gustina, A.S., and M.C. Trudeau. 2011. hERG potassium channel gating is mediated by N- and C-terminal region interactions. *J. Gen. Physiol.* 137:315–325. https://doi.org/10.1085/jgp.201010582

Gustina, A.S., and M.C. Trudeau. 2012. HERG potassium channel regulation by the N-terminal eag domain. *Cell. Signal.* 24:1592–1598. https://doi.org/10.1016/j.cellsig.2012.04.004

Haddad, G.A., and R. Blunck. 2011. Mode shift of the voltage sensors in Shaker K^+ channels is caused by energetic coupling to the pore domain. *J. Gen. Physiol.* 137:455–472. https://doi.org/10.1085/jgp.201010573

Hardman, R.M., P.J. Stansfeld, S. Dalibalta, M.J. Sutcliffe, and J.S. Mitcheson. 2007. Activation gating of hERG potassium channels: S6 glycines are not required as gating hinges. *J. Biol. Chem.* 282:31972–31981. https://doi.org/10.1074/jbc.M705835200

Ho, W.K., I. Kim, C.O. Lee, and Y.E. Earm. 1998. Voltage-dependent blockade of HERG channels expressed in Xenopus oocytes by external Ca^{2+} and Mg^{2+}. *J. Physiol.* 507:631–638. https://doi.org/10.1111/j.1469-7793.1998.631bs.x

Hull, C.M., S. Sokolov, A.C. Van Slyke, and T.W. Claydon. 2014. Regional flexibility in the S4-S5 linker regulates hERG channel closed-state stabilization. *Pflugers Arch.* 466:1911–1919. https://doi.org/10.1007/s00424-013-1431-9

Islas, L.D. 2016. Functional diversity of potassium channel voltage-sensing domains. *Channels (Austin).* 10:202–213. https://doi.org/10.1080/19336950.2016.1141842

Jiang, M., W. Dun, and G.N. Tseng. 1999. Mechanism for the effects of extracellular acidification on HERG-channel function. *Am. J. Physiol.* 277:H1283–H1292.

Johnson, J.P. Jr., J.R. Balser, and P.B. Bennett. 1999a. Enhancement of HERG K^+ currents by Cd^{2+} destabilization of the inactivated state. *Biophys. J.* 77:2534–2541. https://doi.org/10.1016/S0006-3495(99)77088-8

Johnson, J.P. Jr., F.M. Mullins, and P.B. Bennett. 1999b. Human ether-à-go-go-related gene K^+ channel gating probed with extracellular ca^{2+}. Evidence for two distinct voltage sensors. *J. Gen. Physiol.* 113:565–580. https://doi.org/10.1085/jgp.113.4.565

Johnson, J.P. Jr., J.R. Balser, and P.B. Bennett. 2001. A novel extracellular calcium sensing mechanism in voltage-gated potassium ion channels. *J. Neurosci.* 21:4143–4153. https://doi.org/10.1523/JNEUROSCI.21-12-04143.2001

Kazmierczak, M., X. Zhang, B. Chen, D.K. Mulkey, Y. Shi, P.G. Wagner, K. Pivaroff-Ward, J.K. Sassic, D.A. Bayliss, and T. Jegla. 2013. External pH modulates EAG superfamily K^+ channels through EAG-specific acidic residues in the voltage sensor. *J. Gen. Physiol.* 141:721–735. https://doi.org/10.1085/jgp.201210938

Kuzmenkin, A., F. Bezanilla, and A.M. Correa. 2004. Gating of the bacterial sodium channel, NaChBac: voltage-dependent charge movement and gating currents. *J. Gen. Physiol.* 124:349–356. https://doi.org/10.1085/jgp.200409139

Labro, A.J., J.J. Lacroix, C.A. Villalba-Galea, D.J. Snyders, and F. Bezanilla. 2012. Molecular mechanism for depolarization-induced modulation of Kv channel closure. *J. Gen. Physiol.* 140:481–493. https://doi.org/10.1085/jgp.201210817

Lacroix, J.J., A.J. Labro, and F. Bezanilla. 2011. Properties of deactivation gating currents in Shaker channels. *Biophys. J.* 100:L28–L30. https://doi.org/10.1016/j.bpj.2011.01.043

Lin, M.C.A., and D.M. Papazian. 2007. Differences between ion binding to eag and HERG voltage sensors contribute to differential regulation of activation and deactivation gating. *Channels (Austin).* 1:429–437. https://doi.org/10.4161/chan.1.6.5760

Liu, J., M. Zhang, M. Jiang, and G.-N. Tseng. 2003. Negative charges in the transmembrane domains of the HERG K channel are involved in the activation- and deactivation-gating processes. *J. Gen. Physiol.* 121:599–614. https://doi.org/10.1085/jgp.200308788

Lörinczi, É., J.C. Gómez-Posada, P. de la Peña, A.P. Tomczak, J. Fernández-Trillo, U. Leipscher, W. Stühmer, F. Barros, and L.A. Pardo. 2015. Voltage-dependent gating of KCNH potassium channels lacking a covalent link be-

tween voltage-sensing and pore domains. *Nat. Commun.* 6:6672. https://doi.org/10.1038/ncomms7672

Lu, Y., M.P. Mahaut-Smith, A. Varghese, C.L.H. Huang, P.R. Kemp, and J.I. Vandenberg. 2001. Effects of premature stimulation on HERG K(+) channels. *J. Physiol.* 537:843–851. https://doi.org/10.1113/jphysiol.2001.012690

Morais Cabral, J.H., A. Lee, S.L. Cohen, B.T. Chait, M. Li, and R. Mackinnon. 1998. Crystal structure and functional analysis of the HERG potassium channel N terminus: a eukaryotic PAS domain. *Cell.* 95:649–655. https://doi.org/10.1016/S0092-8674(00)81635-9

Ng, C.A., M.J. Hunter, M.D. Perry, M. Mobli, Y. Ke, P.W. Kuchel, G.F. King, D. Stock, and J.I. Vandenberg. 2011. The N-terminal tail of hERG contains an amphipathic α-helix that regulates channel deactivation. *PLoS One.* 6:e16191. https://doi.org/10.1371/journal.pone.0016191

Ng, C.A., M.D. Perry, P.S. Tan, A.P. Hill, P.W. Kuchel, and J.I. Vandenberg. 2012. The S4-S5 linker acts as a signal integrator for HERG K+ channel activation and deactivation gating. *PLoS One.* 7:e31640. https://doi.org/10.1371/journal.pone.0031640

Ng, C.A., K. Phan, A.P. Hill, J.I. Vandenberg, and M.D. Perry. 2014. Multiple interactions between cytoplasmic domains regulate slow deactivation of Kv11.1 channels. *J. Biol. Chem.* 289:25822–25832. https://doi.org/10.1074/jbc.M114.558379

Orchard, C.H., and H.E. Cingolani. 1994. Acidosis and arrhythmias in cardiac muscle. *Cardiovasc. Res.* 28:1312–1319. https://doi.org/10.1093/cvr/28.9.1312

Papazian, D.M., X.M. Shao, S.A. Seoh, A.F. Mock, Y. Huang, and D.H. Wainstock. 1995. Electrostatic interactions of S4 voltage sensor in Shaker K+ channel. *Neuron.* 14:1293–1301. https://doi.org/10.1016/0896-6273(95)90276-7

Piper, D.R., A. Varghese, M.C. Sanguinetti, and M. Tristani-Firouzi. 2003. Gating currents associated with intramembrane charge displacement in HERG potassium channels. *Proc. Natl. Acad. Sci. USA.* 100:10534–10539. https://doi.org/10.1073/pnas.1832721100

Piper, D.R., J. Rupp, F.B. Sachse, M.C. Sanguinetti, and M. Tristani-Firouzi. 2008. Cooperative interactions between R531 and acidic residues in the voltage sensing module of hERG1 channels. *Cell. Physiol. Biochem.* 21:37–46. https://doi.org/10.1159/000113745

Priest, M.F., J.J. Lacroix, C.A. Villalba-Galea, and F. Bezanilla. 2013. S3-S4 linker length modulates the relaxed state of a voltage-gated potassium channel. *Biophys. J.* 105:2312–2322. https://doi.org/10.1016/j.bpj.2013.09.053

Ramsey, I.S., Y. Mokrab, I. Carvacho, Z.A. Sands, M.S.P. Sansom, and D.E. Clapham. 2010. An aqueous H+ permeation pathway in the voltage-gated proton channel Hv1. *Nat. Struct. Mol. Biol.* 17:869–875. https://doi.org/10.1038/nsmb.1826

Sanguinetti, M.C., and Q.P. Xu. 1999. Mutations of the S4-S5 linker alter activation properties of HERG potassium channels expressed in Xenopus oocytes. *J. Physiol.* 514:667–675. https://doi.org/10.1111/j.1469-7793.1999.667ad.x

Sanguinetti, M.C., C. Jiang, M.E. Curran, and M.T. Keating. 1995. A mechanistic link between an inherited and an acquired cardiac arrhythmia: HERG encodes the IKr potassium channel. *Cell.* 81:299–307. https://doi.org/10.1016/0092-8674(95)90340-2

Sanguinetti, M.C., M.E. Curran, P.S. Spector, and M.T. Keating. 1996. Spectrum of HERG K+-channel dysfunction in an inherited cardiac arrhythmia. *Proc. Natl. Acad. Sci. USA.* 93:2208–2212. https://doi.org/10.1073/pnas.93.5.2208

Santiago-Castillo, J.A., M. Covarrubias, J.E. Sánchez-Rodríguez, P. Perez-Cornejo, and J. Arreola. 2010. Simulating complex ion channel kinetics with IonChannelLab. *Channels (Austin).* 4:422–428. https://doi.org/10.4161/chan.4.5.13404

Shi, Y.P., Y.M. Cheng, A.C. Van Slyke, and T.W. Claydon. 2014. External protons destabilize the activated voltage sensor in hERG channels. *Eur. Biophys. J.* 43:59–69. https://doi.org/10.1007/s00249-013-0940-y

Silverman, W.R., C.Y. Tang, A.F. Mock, K.B. Huh, and D.M. Papazian. 2000. Mg(2+) modulates voltage-dependent activation in ether-à-go-go potassium channels by binding between transmembrane segments S2 and S3. *J. Gen. Physiol.* 116:663–678. https://doi.org/10.1085/jgp.116.5.663

Smith, P.L., T. Baukrowitz, and G. Yellen. 1996. The inward rectification mechanism of the HERG cardiac potassium channel. *Nature.* 379:833–836. https://doi.org/10.1038/379833a0

Spector, P.S., M.E. Curran, A. Zou, M.T. Keating, and M.C. Sanguinetti. 1996. Fast inactivation causes rectification of the IKr channel. *J. Gen. Physiol.* 107:611–619. https://doi.org/10.1085/jgp.107.5.611

Subbiah, R.N., C.E. Clarke, D.J. Smith, J. Zhao, T.J. Campbell, and J.I. Vandenberg. 2004. Molecular basis of slow activation of the human *ether-a-go-go* related gene potassium channel. *J. Physiol.* 558:417–431. https://doi.org/10.1113/jphysiol.2004.062588

Swartz, K.J. 2008. Sensing voltage across lipid membranes. *Nature.* 456:891–897. https://doi.org/10.1038/nature07620

Tan, P.S., M.D. Perry, C.A. Ng, J.I. Vandenberg, and A.P. Hill. 2012. Voltage-sensing domain mode shift is coupled to the activation gate by the N-terminal tail of hERG channels. *J. Gen. Physiol.* 140:293–306. https://doi.org/10.1085/jgp.201110761

Tao, X., A. Lee, W. Limapichat, D.A. Dougherty, and R. MacKinnon. 2010. A Gating Charge Transfer Center in Voltage Sensors. *Science.* 328:67–73.

Terai, T., T. Furukawa, Y. Katayama, and M. Hiraoka. 2000. Effects of external acidosis on HERG current expressed in Xenopus oocytes. *J. Mol. Cell. Cardiol.* 32:11–21. https://doi.org/10.1006/jmcc.1999.1048

Thouta, S., C.M. Hull, Y.P. Shi, V. Sergeev, J. Young, Y.M. Cheng, and T.W. Claydon. 2017. Stabilization of the Activated hERG Channel Voltage Sensor by Depolarization Involves the S4-S5 Linker. *Biophys. J.* 112:300–312. https://doi.org/10.1016/j.bpj.2016.12.021

Van Slyke, A.C., S. Rezazadeh, M. Snopkowski, P. Shi, C.R. Allard, and T.W. Claydon. 2010. Mutations within the S4-S5 linker alter voltage sensor constraints in hERG K+ channels. *Biophys. J.* 99:2841–2852. https://doi.org/10.1016/j.bpj.2010.08.030

Van Slyke, A.C., Y.M. Cheng, P. Mafi, C.R. Allard, C.M. Hull, Y.P. Shi, and T.W. Claydon. 2012. Proton block of the pore underlies the inhibition of hERG cardiac K+ channels during acidosis. *Am. J. Physiol. Cell Physiol.* 302:C1797–C1806. https://doi.org/10.1152/ajpcell.00324.2011

Villalba-Galea, C.A. 2014. Hv1 proton channel opening is preceded by a voltage-independent transition. *Biophys. J.* 107:1564–1572. https://doi.org/10.1016/j.bpj.2014.08.017

Villalba-Galea, C.A., W. Sandtner, D.M. Starace, and F. Bezanilla. 2008. S4-based voltage sensors have three major conformations. *Proc. Natl. Acad. Sci. USA.* 105:17600–17607. https://doi.org/10.1073/pnas.0807387105

Wang, W., and R. MacKinnon. 2017. Cryo-EM Structure of the Open Human Ether-à-go-go-Related K+ Channel hERG. *Cell.* 169:422–430.e10. https://doi.org/10.1016/j.cell.2017.03.048

Wang, J., M.C. Trudeau, A.M. Zappia, and G.A. Robertson. 1998. Regulation of deactivation by an amino terminal domain in human ether-à-go-go-related gene potassium channels. *J. Gen. Physiol.* 112:637–647. https://doi.org/10.1085/jgp.112.5.637

Wang, J., C.D. Myers, and G.A. Robertson. 2000. Dynamic control of deactivation gating by a soluble amino-terminal domain in HERG K(+) channels. *J. Gen. Physiol.* 115:749–758. https://doi.org/10.1085/jgp.115.6.749

Xiao, Y.-F., N. Chandler, H. Dobrzynski, E.S. Richardson, E.M. Tenbroek, J.J. Wilhelm, V. Sharma, A. Varghese, M.R. Boyett, P.A. Iaizzo, and D.C. Sigg. 2010. Hysteresis in human HCN4 channels: a crucial feature potentially affecting sinoatrial node pacemaking. *Sheng Li Xue Bao.* 62:1–13.

Zhang, M., J. Liu, and G.-N. Tseng. 2004. Gating charges in the activation and inactivation processes of the HERG channel. *J. Gen. Physiol.* 124:703–718. https://doi.org/10.1085/jgp.200409119

Zhang, M., J. Liu, M. Jiang, D.M. Wu, K. Sonawane, H.R. Guy, and G.N. Tseng. 2005. Interactions between charged residues in the transmembrane segments of the voltage-sensing domain in the hERG channel. *J. Membr. Biol.* 207:169–181. https://doi.org/10.1007/s00232-005-0812-1

Zhou, Q., and G.C.L. Bett. 2010. Regulation of the voltage-insensitive step of HERG activation by extracellular pH. *Am. J. Physiol. Heart Circ. Physiol.* 298:H1710–H1718. https://doi.org/10.1152/ajpheart.01246.2009